PCCP

Accepted Manuscript




ROYAL SOCIETY OF CHEMISTRY

www.rsc.org/pccp

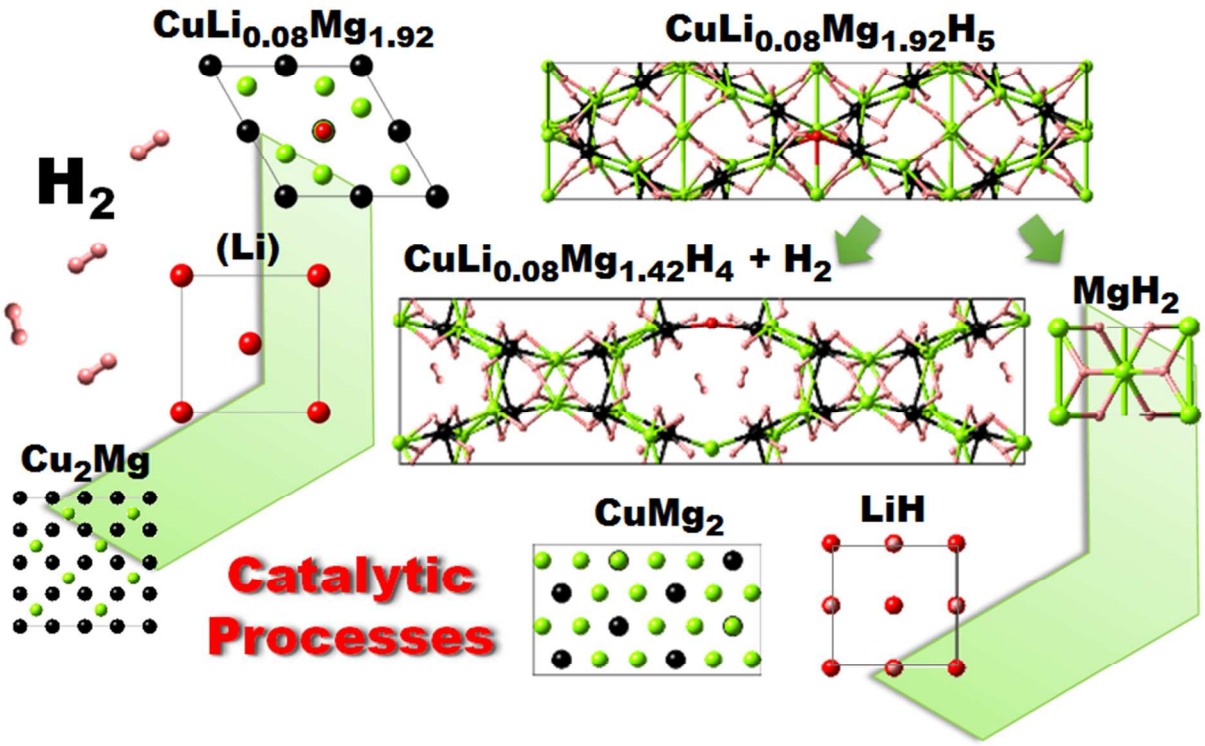


**Cu-Li-Mg-H novel hydrides and catalytic processes will open new vistas in the field of storage for both hydrogen and batteries.**

# The catalytic reactions in the Cu-Li-Mg-H high capacity hydrogen storage system

M. H. Braga[1] and A. El-Azab[2]

[1]CEMUC, Physics Engineering Department, Engineering Faculty, University of Porto, R. Dr. Roberto Frias s/n, 4200-465 Porto, Portugal, E-mail: mbraga@fe.up.pt

[2]School of Nuclear Engineering and School of Materials Engineering, Purdue University, West Lafayette, IN, USA

**Keywords:** metal hydrides, catalysts, hydrogen storage materials, negative electrodes, Cu-Li-Mg-H system.

**Abstract:** A family of hydrides including the high capacity, $MgH_2$ and LiH, is reported. The disadvantages these hydrides normally display (high absorption/desorption temperatures and poor kinetics) are mitigated by Cu-hydrides catalysis. This paper reports on the synthesis of novel $CuLi_{0.08}Mg_{1.42}H_4$ and $CuLi_{0.08}Mg_{1.92}H_5$ hydrides, which are structurally and thermodynamically characterized for the first time. The $CuLi_{0.08}Mg_{1.42}H_4$ hydride structure in nanotubes is able to hold molecular $H_2$, increasing the gravimetric and volumetric capacity of this compound. The catalytic effect these compounds show on hydride formation and decomposition of $CuMg_2$ and $Cu_2Mg/MgH_2$, Li and LiH, Mg and $MgH_2$ is analyzed. The Gibbs energy, decomposition temperature, and gravimetric capacity of the reactions occurring within the Cu-Li-Mg-H system are presented for the first time. First principles and phonon calculations are compared with experiments, including neutron spectroscopy. It is demonstrated that the most advantageous sample contains $CuLi_{0.08}Mg_{1.92}$ and (Li) ~ $Li_2Mg_3$; it desorbs/absorbs hydrogen according to the reaction, $2CuLi_{0.08}Mg_{1.42}H_4 + 2Li + 4MgH_2 \leftrightarrow 2CuLi_{0.08}Mg_{1.92} + Li_2Mg_3 + 8H_2$ at 114 ºC (5.0 wt%) - 1 atm, falling within the Proton Exchange Membrane fuel cells applications window. Finally the reaction $2CuLi_{0.08}Mg_{1.42}H_4 + MgH_2 \leftrightarrow 2CuLi_{0.08}Mg_{1.92} + 5H_2$ at 15 ºC (4.4 wt%) - 1 atm, is found to be the main reaction of the samples containing $CuLi_{0.08}Mg_{1.92}$ that were analyzed in this study.

## 1. Introduction

Our research has led to the discovery of a novel family of hydrides displaying catalytic behavior on the hydrogen absorption/desorption process of $MgH_2$ and LiH. This report provides a detailed analysis of Cu-hydrides catalysis. At this writing, this is the first time that a hydrogenation/catalysis process is directly analyzed using samples of different equilibrium regions of a ternary phase diagram. We use the advantages that chemical equilibrium and phase interconnection provides to optimize the hydrogenation/dehydrogenation processes. A comprehensive set of experiments have been performed in exhaustive detail to understanding the nature and the viability of tailoring this family of hydrides, for deployment within a vast number of applications, as set forth in this document.

Much of the recent research concerning metal hydrides is motivated by the potential to use such materials as hydrogen storage media. In particular, the need for better vehicular hydrogen storage systems has generated high demands on the energy density of storage media. Metal hydrides have a wide variety of applications outside of stationary and vehicular hydrogen storage, e.g., in metal hydride based refrigerators [1], pneumatic actuators [2], heat pump utilizing metal hydrides as solid state compressors [3], hydrogen separation from mixed gas streams and isotopic enrichment [4], metal hydride batteries [5] to name some. Several comprehensive reviews further enumerate numerous other applications of metal hydrides [6,7]. Light metal hydrides, like LiH and $MgH_2$, present high gravimetric (12.7 and 7.7 wt%, respectively) and volumetric hydrogen storage capacities. The synthesis of lithium hydride is rather inconvenient, since it occurs at 689 °C, a temperature at which lithium is in the liquid state [10]. Lithium hydride is an ionic, salt-like, crystalline solid with a high-melting point. Electrochemical studies on LiH were conducted upon recognition that molten LiH conducts electricity [11]. Many other studies were conducted regarding the electrolysis of solid LiH in

which simultaneous cathodic deposition of lithium and anodic evolution of hydrogen was observed [12-16].

In his latest paper, *High Pressure Synthesis of Novel Li-TM Hydrides,* Vajo *et al.*, demonstrated that hydrogen-rich, but strongly bound hydrides, such as LiH, are destabilized by alloying with Si. This destabilization method has been shown to substantially improve their potential, as hydrogen storage materials for fuel cell powered vehicles [17].

Y. Oumellal *et al,* in a recent communication, [18] investigated the use of $MgH_2$ among other hydrides, as enhanced negative electrodes in lithium-conversion batteries. These authors suggested that $MgH_2$ reacts with Li according to: $MgH_2 + 2Li^+ + 2e^- \leftrightarrow Mg + 2LiH$. Pursuing further lithiation, the authors verified that instead of having the coexistence of Mg (h.c.p.) and Li (b.c.c.), only (Li) (b.c.c.) solid solution with Mg dissolved in a Li matrix was present. The latter reaction was found to be reversible as well. Avoiding the formation of (Li), $MgH_2$ electrodes lead to a theoretical discharge capacity of 1500 $mAhg^{-1}$ and to a reversible capacity of 1125 $mAhg^{-1}$ in comparison with 370 $mAhg^{-1}$ for graphite (currently used in commercial Li-ion batteries). Lithium's three dimensional anodes formed from the liquid miscibility gap of the Li-H system were also theoretically studied [19].

The search for on-board hydrogen storage materials has led to a conclusion that a system of four or more elements will most likely be required to cover all specifications. A catalysis and destabilization strategy then becomes a viable, attractive path forward for further progress.

In this work, we assess the potential of the Cu-Li-Mg-H as a hydrogen storage system and for anode applications. We calculate the enthalpy and entropy of formation of each phase and reaction involved in the hydrogenation/dehydrogenation process. Experimental work based on Differential Scanning Calorimetry/Thermo Gravimetry (DSC/TG), X-Ray Diffraction (XRD) and Inelastic Neutron Scattering (INS) is used to validate the theoretical results.

The catalytic effect within the Cu-Li-Mg-H system on hydride formation and decomposition of $CuMg_2$ ($Cu_2Mg/MgH_2$), Mg ($MgH_2$), and Li (LiH) are thoroughly investigated.

In contrast to the previous studies on destabilized reactions, where an element or a compound is added to a hydride to induce a destabilizing effect [20], we demonstrate that the LiH and $MgH_2$ can naturally form at considerably lower temperatures in the Cu-Li-Mg system after hydrogenation. We demonstrate that the temperature at which these hydrides desorb hydrogen in the presence of the $CuLi_{0.08}Mg_{1.42}H_4$ is also substantially lower. The samples used in this regard are summarized in Table 1 and figure 1.

**Table 1.** Equilibrium phase regions in the Cu-Li-Mg system. All of these equilibrium phase regions include $CuLi_{0.08}Mg_{1.92}$ and were at least theoretically studied in this work.

| Studied samples | Phases in Equilibrium | Experimentally studied in this work |
|---|---|---|
| **A** | $Cu_2Mg + CuLi_{0.08}Mg_{1.92}$ | **yes** |
| **B** | $Cu_2Mg + CuLi_{0.08}Mg_{1.92} + CuMg_2$ | **yes** |
| **C** | $(Li) + Cu_2Mg + CuLi_{0.08}Mg_{1.92}$ | **yes** |
| **D** | $(Li) + CuLi_{0.08}Mg_{1.92}$ | **no** |
| **E** | $(Li) + CuLi_{0.08}Mg_{1.92} + CuMg_2$ | **no** |
| **F** | $CuLi_{0.08}Mg_{1.92} + CuMg_2$ | **no** |

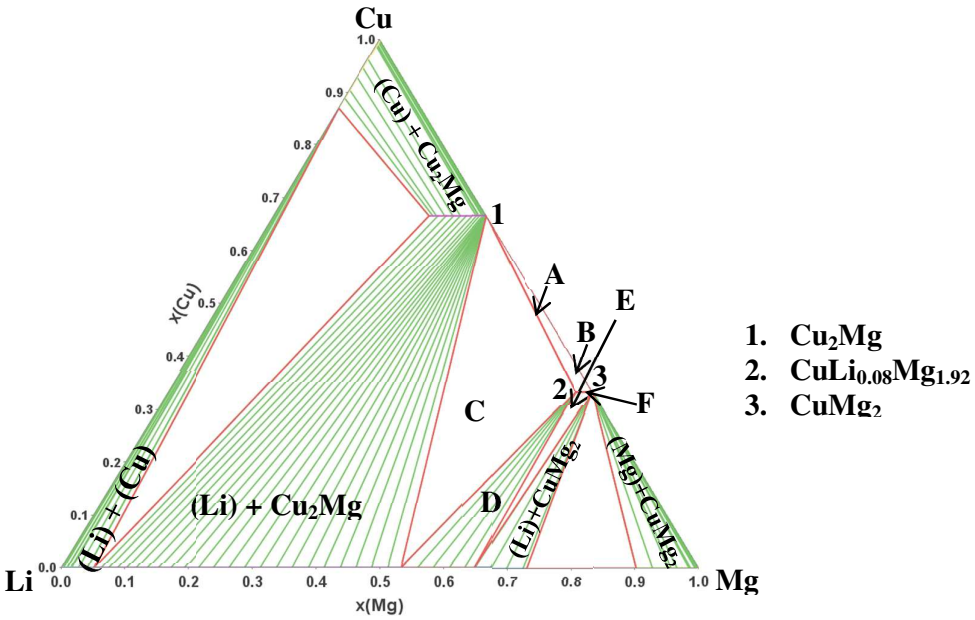


**Fig 1.** Ternary section of the Cu-Li-Mg phase diagram at 25 ºC. The phase diagram was obtained using the parameters of the binaries of COST 507 database in [21] coupled with the thermodynamic data obtained for $CuLi_{0.08}Mg_{1.92}$. Phase regions corresponding to samples A to E were highlighted in the diagram and included in Table 1.

## 2. Experimental

Samples from three different phase regions of the Cu-Li-Mg system were synthesized and studied using different experimental techniques. The goal was to validate the reactions taking place upon hydrogenation/dehydrogenation which were predicted in this work (Table 2).

### 2.1 Cu-Li-Mg-H. Synthesis of samples A and B

A Cu-Li-Mg alloy was prepared by melting the elements together: Cu (electrolytic, 99.99% purity, 325 mesh), Mg (99.8% purity, 200 mesh, Alfa Aesar), and small (less than 3mm) pieces of Li (99% purity, Alfa Aesar), at 850 °C and up to 1200 ºC for 1 h using stainless steel crucible and fittings and a stirring device. The alloy was solidified by quenching into liquid nitrogen or by cooling down. Samples were firstly characterized by means of XRD using a Rigaku Ultima III powder diffractometer, and their compositions were roughly determined by

means of the Match software [23] which uses the Reference Intensity Ratio (RiR) method [24] to obtain the phase fractions. Patterns were collected with CuKα typically from 2θ values in the range of 15° to 70° with steps of 0.02° and a counting time of 10 s per bin.

Part of the resulting mixture was then divided into portions. Some portions were sealed inside a stainless steel crucible and heated up to 200 °C and kept at this temperature under $H_2$ at pressures that vary from 15 atm to 109 atm for 1h. In most cases, the pressures were initially around 100 atm. Samples were not activated nor heat treated prior to this treatment. Some of these samples were then cooled to -263 °C to be measured on FDS - the neutron vibrational spectroscopy instrument - or to room temperature to be measured by means of laboratory XRD or DSC/TG.

2.2 Cu-Li-Mg-H. Synthesis of samples C

A Cu-Li-Mg alloy was prepared by melting the elements together: Cu, Mg and Li, at 550 °C for 1 h followed by 1100 °C for 1h using similar elements, crucibles and instruments described in 2.1 above. The alloy was quenched into liquid nitrogen. The resulting samples had 25.0 at% of $CuLi_{0.08}Mg_{1.92}$, 4.6 at% of $Cu_2Mg$ and 70.4 at% of (Li) ~ $Li_2Mg_3$. The resulting mixture was then sealed inside a stainless steel crucible and kept at 200 °C for 17 h under $H_2$ at 60 atm. The samples were characterized by means of XRD, DSC/TG and INS before and after hydrogenation.

2.3 Differential Scanning Calorimetry (DSC) / Thermo Gravimetric (TG)

DSC/TG measurements were performed under Ar flux of 27 ml/min with a Netzsch instrument (STA 449C) from room temperature up to 450 °C or higher, using alumina pans and lids and different heating rates (5 and 10 °C/min).

2.4 X-ray diffraction (XRD)

Phases were determined and analyzed by means of XRD using a Rigaku Ultima III powder diffractometer. Patterns were collected with CuKα typically from 2θ from 15 to 70° with steps of 0.02° and a counting time of 10 s per bin.

Synchrotron XRD was additionally performed with sample A at 11-BM, APS, Argonne (λ = 0.413570 Å). Sample A was grinded, hydrogenated as previously described, and introduced in a quartz capillary that was sealed.

XRD diffraction patterns were refined using Le Bail and Rietveld methods.

2.5 Incoherent inelastic neutron scattering (INS)

Neutron vibrational spectroscopy characterization was performed with samples from the Cu-Mg, Cu-Li-Mg, and Cu-Li-Mg-H systems at -263 °C. The Filter Difference Spectrometer (FDS) at the Los Alamos Neutron Scattering Center, USA, was used for this purpose. Samples of the Ni-Mg system were also analyzed for comparison. The background of the pristine sample was always subtracted from the hydrogenated sample vibration spectra to highlight the hydrogen vibration modes.

## 3. Theoretical

The theoretical studies allowed us to establish all the reactions in Table 2 as well as complex catalytic processes occurring within the system. These processes and properties of the system were validated by the experimental work.

Density Functional Theory (DFT) [25-27] has been used to predict structure and properties of the alloy systems of interest in the current work. Projector Augmented Wave (PAW) pseudopotentials [28] and the Perdew–Burke–Ernzerhof (PBE) functional [26] were used as implemented in the Vienna *Ab Initio* Simulation Package (VASP) code [29]. A plane wave

cutoff of at least 355.18 eV, and k-spacings of 0.230 x 0.230 x 0.230 $Å^{-1}$ were used. Calculations were done in the real space and were performed with *P2* space group supercells containing at least 64 atoms (8 atoms of Cu, 15 of Mg, 1 of Li and 40 of H) and 104 (16 atoms of Cu, 23 of Mg, 1 of Li and 64 of H). The supercells contained as many atoms as possible to allow better approximations with the real Li concentrations. The total energy was minimized with respect to the volume (volume relaxation), the shape of the unit cell (cell external relaxation), and the position of the atoms within the cell (cell internal relaxation).

In the case of Li, Mg, $Cu_2Mg$, $CuMg_2$, LiH and $MgH_2$, calculations were executed in the reciprocal space using the elements or compounds primitive cells. We have further optimized the $H_2$ molecule "in a box". For the $H_2$ molecule, a cubic box of $10^3$ $Å^3$ was used with a plane wave cutoff of 900 eV, and k-mesh of 8×8×8.

The Phonon direct method [30] was used to predict the lattice dynamics using the quasi-harmonic approximation on VASP minimized structures that had the lowest ground state energy. This enabled the calculation of the formation energy (of the electronic configuration) at ground state using VASP. Zero point energy, phonons' energy and the entropy were calculated using the Phonon code [30]. We have actually calculated the Helmholtz free energy, which approximates the Gibbs free energy at zero stress.

The Helmholtz free energy, the internal energy which is used here to approximate the enthalpy, and the entropy were calculated after the vibration frequencies, ω, as follows:

$$F_{phonon} = 3Nk_BT\int_0^{\omega_L} ln\left(2sinh\frac{\hbar\omega}{2k_BT}\right)g(\omega)d\omega \quad (1)$$

$$E_{phonon} = 3N\frac{\hbar}{2}\int_0^{\omega_L} \omega coth\left(\frac{\hbar\omega}{2k_BT}\right)g(\omega)d\omega \quad (2)$$

$$S_{phonon} = 3Nk_B\int_0^{\omega_L}\left[\frac{\hbar\omega}{2k_BT}coth\left(\frac{\hbar\omega}{2k_BT}\right) - ln\left(2sinh\frac{\hbar\omega}{2k_BT}\right)\right]g(\omega)d\omega \quad (3)$$

where $N$ is the number of atoms in the cell, $k_B$ is Boltzmann's constant, $T$ the absolute temperature, $\omega_L$ the maximal frequency and $g(\omega)$ the frequency distribution function. Therefore, by adding the electronic contribution, $E_{elec}$, calculated using DFT as implemented in VASP, the zero-point energy of the quantum harmonic oscillator, $ZPE = E(0\ K) = \frac{1}{2}\hbar\omega$, and the phonon contribution, the total internal energy $E(T) = E_{elec} + ZPE + E_{phonon}(T)$ is obtained. The Helmholtz free energy, $F(T)$, is given by $F(T) = E(T) - TS(T)$ in which $S(T) = S_{phonon}(T)$ is the vibrational entropy at the absolute temperature $T$. The Helmholtz free energy was considered to be equal to the Gibbs free energy since the PV term (in which P is the pressure and V the volume) can be neglected for solids in the conditions mentioned before.

For the molecule of $H_2$, besides the VASP-optimized total energy, $E_{elec}$, phonons were used to calculate the vibration energy: $E_{vib}$ ($H_2$) = $\hbar\omega_0 n(\omega_0)$. The energy related with the $PV$ term that cannot be neglected in an ideal gas, $PV = k_BT$, and the energy related with the other degrees of freedom of the molecule (the sum of its translational energy, $(3/2)k_BT$, and its rotational energy, $k_BT$) were also included in the term, $(7/2)RT$, valid for a mole of molecules, in which R is the ideal gas constant. The obtained results were compared with NIST's gas phase thermochemistry data [31].

## 4. Results and Discussion

In this section we discuss in detail the parent ternary phase, $CuLi_{0.08}Mg_{1.92}$, its hydrides: $CuLi_{0.08}Mg_{1.42}H_4$ and $CuLi_{0.08}Mg_{1.92}H_5$, and the reactions occurring upon hydrogenation/dehydrogenation and shown in Table 2. For validating the latter reactions, it was performed a detailed analysis of the results obtained with each sample of Table 1 and figure 1.

4.1 The Cu-Li-Mg system and subsystems

The pioneering work of Reilly and Wiswall [32] on hydrogen storage in $CuMg_2$ provides the first clear example of a destabilization reaction. $CuMg_2 + (3/2)H_2$ were formed from $(3/2)MgH_2 + (1/2)Cu_2Mg$ at an equilibrium pressure of 1 atm, at 240 °C. This temperature is approximately 40 °C lower than required for releasing $H_2$ from pure $MgH_2$ at 1 atm. However, since $CuMg_2$ does not form a hydride, this work was set aside until recently [33].

$CuMg_2$ crystallizes with an orthorhombic structure *Fddd*; nonetheless, the only ternary compound in the Cu-Li-Mg system, $CuLi_xMg_{2-x}$ (x = 0.08), crystallizes with a hexagonal structure $P6_222$, just like $NiMg_2$, a compound known for its ability to store hydrogen.

Conversely, $NiMg_2$ forms $NiMg_{2-x}Sn_x$ (with x = 0.22 and 0.40 and the replacement of Mg by Sn produces changes in the structure of $NiMg_2$, wherein the alloy changes from the $NiMg_2$-type (hexagonal) to the $CuMg_2$-type (orthorhombic) [34]. $NiMg_2$ absorbs up to 3.6 wt% of hydrogen, at 1 atm and 282 °C forming the hydride, $NiMg_2H_4$. In spite of the fact that the percentage of $H_2$ absorbed by $NiMg_2$ is enough to warrant practical applications, the temperature at which the alloy desorbs hydrogen is much too high for current applications. Nonetheless, the alloy can be found in practical applications when added to other elements/alloys e.g. Ni-MH battery negative electrodes.

A comparison between the phase diagrams of the Cu-Mg and Ni-Mg systems reveals that these binary systems form compounds with similar stoichiometry [35]. $NiMg_2$ is formed by peritectic reaction of the elements at 759 °C and $CuMg_2$ at 568 °C by congruent melting. The presence of Li lowers even further the melting point of $CuMg_2$ [36].

Since the enthalpy of formation of the hydride is related to that of the primary alloy, it was hypothesized that $CuLi_{0.08}Mg_{1.92}$ might have practical applications as a hydrogen storage material. $CuLi_{0.08}Mg_{1.92}$ would rather have a $NiMg_2$-type, instead of a $CuMg_2$-type, of hydrogen storage behavior since its crystal structure is closer to $NiMg_2$. The current work confirms that

hypothesis and establishes that $CuLi_{0.08}Mg_{1.92}$ forms $CuLi_{0.08}Mg_{1.42}H_4$ and $CuLi_{0.08}Mg_{1.92}H_5$ with a $NiMg_2H_4$ (low temperature allotrope) similar crystal structure.

4.2 The Cu-Li-Mg hydrides

Our studies showed that $CuLi_xMg_{2-x}$ (x = 0.08) absorbs at least 4.4 wt% of $H_2$, corresponding to the formation of $CuLi_{0.08}Mg_{1.42}H_4 + (1/2)MgH_2$ at 15 ºC – 1 atm (Table 2) or $CuLi_{0.08}Mg_{1.92}H_5$ [37] at -80 ºC – 1 atm (Table 2 and figure 2a). Determination of the structures of such compounds is thus important. DFT calculations for several quaternary Cu-Li-Mg-H compounds with different compositions show that the primary phase of $CuLi_{0.08}Mg_{1.92}$-H is $CuLi_{0.08}Mg_{1.92}H_5 = ½([CuH_4]_2Mg_{3-0.16}Li_{0.16}.MgH_2)$ of the type $M_m^{\delta+}[TH_n]^{\delta-}M_o^{\delta+}H^-_p$ (with $M_m$ = $Mg_{3-0.16}Li_{0.16}$, $[TH_n] = [CuH_4]$, $M_o$ = Mg) as it can be observed in figure 2a. These 'composite' hydrides are of a particular interest because they combine two different types of metal–hydrogen bonding in the same structure, for Cu ($[CuH_4]^{3-}$) and Mg ($MgH_2$). The compound $CuLi_{0.08}Mg_{1.92}H_5$ has a monoclinic, *P121* structure, with *a = 30.74 Å, b = 7.31 Å, c = 6.25 Å, α = γ = 90º* and *β = 114.7º* ($Cu_{16}LiMg_{31}H_{80}$) lattice parameters.

Yvon and Renaudin [39] showed that $Ba_7Cu_3H_{17}$, the other known Cu hydride, contains 18-electron tetrahedral complexes, $[CuH_4]^{3-}$. Ni and Zn hydrides contain exactly the same type of tetrahedral complexes, $[NiH_4]^{4-}$ (e.g. $NiMg_2H_4$, $MMgNiH_4$ with M = Ca, Sr, Eu,Yb and $MMgNi_4H_{\sim 4}$ with M = La, Nd, $LaMg_2NiH_7$), and $[ZnH_4]^{2-}$ (e.g. $M_2ZnH_4$ with M = K, Rb, Cs and $M_3ZnH_5$ with M = K, Rb, Cs). In this work, we confirm that Cu forms $[CuH_4]^{3-}$ in $CuLi_{0.08}Mg_{1.92}H_5 = ½([CuH_4]_2Mg_{3-0.16}Li_{0.16}.MgH_2)$ and $CuLi_{0.08}Mg_{1.42}H_4 = ½([CuH_4]_2Mg_{3-0.16}Li_{0.16})$.

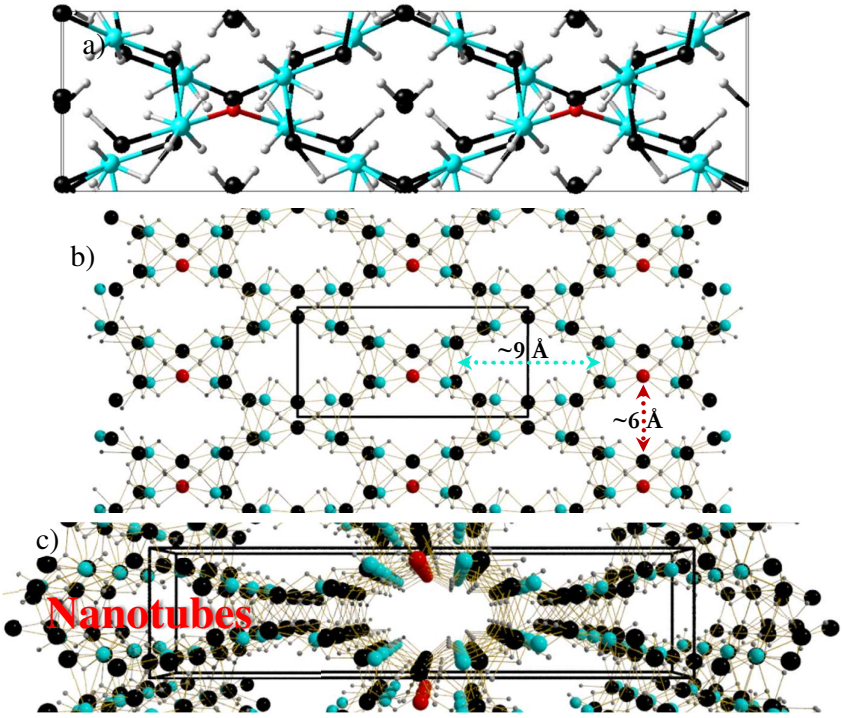


**Fig. 2** Crystal structures of $CuLi_{0.08}Mg_{1.92}H_5$ and $CuLi_{0.08}Mg_{1.42}H_4$. **a)** Crystal structure of $CuLi_{0.08}Mg_{1.92}H_5$ hydride, monoclinic *P121*, of the type ½($[CuH_4]_2Mg_{3-0.16}Li_{0.16}.MgH_2$) and with lattice parameters $a = 30.74$ Å, $b = 7.31$ Å, $c = 6.25$ Å, $\alpha = \gamma = 90^o$ and $\beta = 114.7^o$ ($Cu_{16}LiMg_{31}H_{80}$). **b)** Crystal structure of the $CuLi_{0.08}Mg_{1.42}H_4$ hydride ½($[CuH_4]_2Mg_{3-0.16}Li_{0.16}$) with a zeolite-like structure forming nanotubes with elliptical cross sections with $a = 9$ Å and $b = 6$ Å diameters. The structure is projected in the [100] direction. **c)** The lattice parameters for $CuLi_{0.08}Mg_{1.42}H_4$ are $a = 31.17$ Å, $b = 7.44$ Å, $c = 5.18$ Å, $\alpha = \gamma = 90^o$ and $\beta = 91.11^o$ ($Cu_{16}LiMg_{23}H_{64}$). The structure is projected in the [001] direction. This structure differs from $CuLi_{0.08}Mg_{1.92}H_5$ for not having the hollow's central molecule of $MgH_2$.

**Table 2.** Calculated temperature, enthalpy and entropy of the reactions that may occur with samples from Table 1, above 0 ºC, during a DSC desorption experiment (heating experiment).

| Sample | | Reactions occurring during a DSC experiment after *ex situ* hydrogenation | Temperature, wt.% [ºC; wt.%] | ΔH [kJ/mol $H_2$] | ΔS [kJ/(K.mol $H_2$)] |
|---|---|---|---|---|---|
| **A. B. F.** | **1.** | $2CuLi_{0.08}Mg_{1.42}H_4 + MgH_2 \leftrightarrow 2CuLi_{0.08}Mg_{1.92} + 5H_2$ | 15; 4.4 | 35.3 | 0.123 |
| | **2.** | $2CuLi_{0.08}Mg_{1.42}H_4 + 4MgH_2 + Cu_2Mg \leftrightarrow 2CuLi_{0.08}Mg_{1.92} + 3CuMg_2 + 8H_2$ | 116; 2.8 (a) | 49.6 | 0.127 |
| | **3.** | $Cu_2Mg + 3MgH_2 \leftrightarrow 2CuMg_2 + 3H_2$ | 279; 2.6 | 73.5 | 0.130 |
| | **4.** | $MgH_2 \leftrightarrow Mg + H_2$ | 334; 7.7 | 80.0 | 0.132 |
| **C.** | **1.** | $2CuLi_{0.08}Mg_{1.42}H_4 + MgH_2 \leftrightarrow 2CuLi_{0.08}Mg_{1.92} + 5H_2$ | 15; 4.4 | 35.3 | 0.123 |
| | **2.** | $4MgH_2 + Cu_2Mg + Li_2Mg_3 \leftrightarrow 2CuMg_2 + 2LiH + 4Mg + 3H_2$ | 73; 1.8 | 43.3 | 0.125 |
| | **3.** | $2CuLi_{0.08}Mg_{1.42}H_4 + 2LiH + 2CuMg_2 + Mg \leftrightarrow 2CuLi_{0.08}Mg_{1.92} + Cu_2Mg + Li_2Mg_3 + 5H_2$ | 177; 2.1 (b,c) | 58.6 | 0.130 |
| | | $2CuLi_{0.08}Mg_{1.42}H_4 + 2LiH + 2CuMg_2 + MgH_2 \leftrightarrow 2CuLi_{0.08}Mg_{1.92} + Cu_2Mg + Li_2Mg_3 + 6H_2$ | 203; 2.6 | 62.2 | 0.131 |
| | **4.** | $2Li + 3MgH_2 \leftrightarrow Li_2Mg_3 + 3H_2$ | 271; 6.5 | 71.2 | 0.131 |
| | **5.** | $Cu_2Mg + 3MgH_2 \leftrightarrow 2CuMg_2 + 3H_2$ | 279; 2.6 | 73.5 | 0.130 |
| | **6.** | $MgH_2 \leftrightarrow Mg + H_2$ | 334; 7.7 | 80.0 | 0.132 |
| **D.** | **1.** | $2CuLi_{0.08}Mg_{1.42}H_4 + MgH_2 \leftrightarrow 2CuLi_{0.08}Mg_{1.92} + 5H_2$ | 15; 4.4 | 35.3 | 0.123 |
| | **2.** | $2CuLi_{0.08}Mg_{1.42}H_4 + 2Li + 4MgH_2 \leftrightarrow 2CuLi_{0.08}Mg_{1.92} + Li_2Mg_3 + 8H_2$ | 114; 5.0 | 49.6 | 0.128 |
| | | $2CuLi_{0.08}Mg_{1.42}H_4 + 2LiH + 3MgH_2 \leftrightarrow 2CuLi_{0.08}Mg_{1.92} + Li_2Mg_3 + 6H_2$ | 175; 3.8 | 57.9 | 0.129 |
| | | $2CuLi_{0.08}Mg_{1.42}H_4 + 2LiH + 4MgH_2 \leftrightarrow 2CuLi_{0.08}Mg_{1.92} + Li_2Mg_3 + 9H_2$ | 229; 5.6 | 65.2 | 0.130 |
| | **3.** | $2Li + 3MgH_2 \leftrightarrow Li_2Mg_3 + 3H_2$ | 271; 6.5 | 71.2 | 0.131 |
| **E.** | **1.** | $2CuLi_{0.08}Mg_{1.42}H_4 + MgH_2 \leftrightarrow 2CuLi_{0.08}Mg_{1.92} + 5H_2$ | 15; 4.4 | 35.3 | 0.123 |
| | **2.** | $4MgH_2 + Cu_2Mg + Li_2Mg_3 \leftrightarrow 2CuMg_2 + 2LiH + 4Mg + 3H_2$ | 73; 1.8 | 43.3 | 0.125 |
| | **3.** | $2CuLi_{0.08}Mg_{1.42}H_4 + Cu_2Mg + 2Li + 4MgH_2 + 3Mg \leftrightarrow 2CuLi_{0.08}Mg_{1.92} + 2CuMg_2 + Li_2Mg_3 + 8H_2$ | 92; 2.9 (b,c) | 46.3 | 0.127 |
| | | $2CuLi_{0.08}Mg_{1.42}H_4 + Cu_2Mg + 2Li + 7MgH_2 \leftrightarrow 2CuLi_{0.08}Mg_{1.92} + 2CuMg_2 + Li_2Mg_3 + 11H_2$ | 160; 4.0 | 55.5 | 0.128 |
| | | $2CuLi_{0.08}Mg_{1.42}H_4 + Cu_2Mg + 2LiH + 4MgH_2 + 3Mg \leftrightarrow 2CuLi_{0.08}Mg_{1.92} + 2CuMg_2 + Li_2Mg_3 + 9H_2$ | 209; 3.3 | 62.4 | 0.129 |
| | | $2CuLi_{0.08}Mg_{1.42}H_4 + Cu_2Mg + 2LiH + 7MgH_2 \leftrightarrow 2CuLi_{0.08}Mg_{1.92} + 2CuMg_2 + Li_2Mg_3 + 12H_2$ | 241; 4.3 | 66.8 | 0.130 |
| | **4.** | $2Li + 3MgH_2 \leftrightarrow Li_2Mg_3 + 3H_2$ | 271; 6.5 | 71.2 | 0.131 |
| | **5.** | $Cu_2Mg + 3MgH_2 \leftrightarrow 2CuMg_2 + 3H_2$ | 279; 2.6 | 73.5 | 0.130 |
| | **6.** | $MgH_2 \leftrightarrow Mg + H_2$ | 334; 7.7 | 80.0 | 0.132 |

**Note:** The temperatures correspond to theoretical values, therefore, ideal: 0 ºC/min. Besides the decomposition reactions that release hydrogen, $CuLi_{0.08}Mg_{1.92}$ melts at 420 ºC [38] and in the Li-Mg binary system, $Li_2Mg_3 \leftrightarrow$ Liquid + $Li_2Mg_3$ at 557 ºC and Liquid + $Li_2Mg_3 \leftrightarrow$ Liquid at 577 ºC, for x(Li) = 0.40. The reaction $2CuLi_{0.08}Mg_{1.42}H_4 + MgH_2 \leftrightarrow 2CuLi_{0.08}Mg_{1.92}H_5$ it is likely to occur at T < 0 ºC, according to experimental evidences. Nevertheless, calculations of the Gibbs free energies show that $CuLi_{0.08}Mg_{1.42}H_4 + (1/2)MgH_2$ is always more stable than $CuLi_{0.08}Mg_{1.92}H_5$. This difference is small and grows with temperature. $CuLi_{0.08}Mg_{1.92}H_5$ can be formed directly from $CuLi_{0.08}Mg_{1.92}$ and $H_2$ at -80 ºC. [a)]The reaction $2CuLi_{0.08}Mg_{1.42}H_4 + (2/3)CuMg_2 \leftrightarrow 2CuLi_{0.08}Mg_{1.92} + (1/3)Cu_2Mg + 4H_2$ takes place at -50 ºC. [b)]The reaction $4MgH_2 + Cu_2Mg + Li_2Mg_3 \leftrightarrow 2CuMg_2 + 2Li + 4Mg + 4H_2$ takes place at -24 ºC. [c)]The reaction $2CuLi_{0.08}Mg_{1.42}H_4 + 2Li + 2CuMg_2 + Mg \leftrightarrow 2CuLi_{0.08}Mg_{1.92} + Cu_2Mg + Li_2Mg_3 + 4H_2$ takes place at -70 ºC.

According to our theoretical and experimental findings, the structure of $CuLi_{0.08}Mg_{1.42}H_4$ is a zeolite-like [40] crystal structure. It is organized into nanotubes with elliptic cross section with diameters $a$ ~ 6 Å and $b$ ~ 9 Å (figure 2b and 2c). The calculation of the empty space determines that the formula unit $Cu_{16}LiMg_{23}H_{64}$ (for $CuLi_{0.08}Mg_{1.42}H_4$) corresponding to a volume V = 1021.97 $Å^3$ (lattice parameters $a$ = 31.17 Å, $b$ = 7.44 Å, $c$ = 5.18 Å, $\alpha = \gamma = 90º$ and $\beta = 91.11º$) and volume of the holes, $V_{holes}$ ~ 797 $Å^3$, will hold 4 to 8 molecules of $H_2$ resulting on $CuLi_{0.08}Mg_{1.42}H_{4.5}$ and $CuLi_{0.08}Mg_{1.42}H_5$, respectively. Meaning that at 15 ºC a sample of $CuLi_{0.08}Mg_{1.92}$ will be able to desorb 4.8 wt% to 5.2 wt% of hydrogen.

Ultimately, the molecular hydrogen will be released at a different temperature which can eventually be advantageous.

The pressure vs. temperature decomposition range covered by $CuLi_{0.08}Mg_{1.92} + 5H_2 \leftrightarrow CuLi_{0.08}Mg_{1.42}H_4 + (1/2)MgH_2$ falls into DOE's proton exchange membrane (PEM) fuel cell range, 25-120 ºC and 1-10 atm.

*4.2.1 Comparisons with other hydrides*

In DOE's studies [41] alanates ($AlH_4$) are underlined. Alanates have the potential for higher gravimetric hydrogen capacities in the PEM operational window than simple metal hydrides. Alanates can store and release hydrogen reversibly when catalyzed with titanium dopants, according to the following two-step displacive reaction for sodium alanate: $NaAlH_4 \leftrightarrow (1/3)Na_3AlH_6 + (2/3)Al + H_2$ and $Na_3AlH_6 \leftrightarrow 3NaH + Al + (3/2)H_2$. At 1 atm pressure, the first reaction becomes thermodynamically favorable at temperatures above 33°C and can release 3.7 wt% hydrogen, and the second reaction takes place above 110°C and can release 1.8 wt% hydrogen [41]. The total gravimetric yield of the latter reactions together is 5.5 wt% which is very close to the capacity of $CuLi_{0.08}Mg_{1.92}$ - H. Meanwhile the study of the Cu-Li-Mg system as

a hydrogen storage material has just begun and it already shows appealing capacities as a hydrogen storage material.

DOE emphasizes the performance of another complex hydride system based on lithium amide. For this system, the following reversible displacive reaction takes place at 285 °C and 1 atm: $Li_2NH + H_2 \leftrightarrow LiNH_2 + LiH$ [41]. In this reaction, 6.5 wt% of hydrogen can be reversibly stored. However, the current operating temperature is outside of the vehicular operating window. The temperature of this reaction can be lowered to 220 °C with magnesium substitution, albeit at higher pressures [41].

A reaction studied here adds another possibility (please see reaction 4 of samples C and E in Table 2): $2Li + 3MgH_2 \leftrightarrow Li_2Mg_3 + 3H_2$ (6.5 wt%). Although with similar capacity than the lithium amide, it takes place at 271 ºC and 1 atm which is 14 ºC lower than lithium amide.

The only hydrides which are capable of achieving the 9 wt% gravimetric are limited to lithium, boron and aluminum based compounds; at least one of the first-row elements or Al must be added. Proposed hydrides for use in a hydrogen economy include simple hydrides of magnesium [42] or transition metals and complex metal hydrides, typically containing sodium, lithium, or calcium and aluminum or boron. Hydrides chosen for storage applications provide low reactivity (high safety) and high hydrogen storage densities. Leading candidates are lithium hydride, sodium borohydride, lithium aluminum hydride and ammonia borane.

With the $CuLi_{0.08}Mg_{1.92}$ hydrides we explore chemical storage in the metal-hydride as well as physical storage in $CuLi_{0.08}Mg_{1.42}H_4$ taking advantage of its zeolite-like structure in nanotubes. $CuLi_{0.08}Mg_{1.42}H_4$ has a theoretical gravimetric capacity of 3.9 wt% and volumetric density of 89 kg/m$^3$, $CuLi_{0.08}Mg_{1.42}H_{4.5}$ of 4.4 wt% (100 kg/m$^3$) and $CuLi_{0.08}Mg_{1.42}H_5$ of 4.9 wt% (112 kg/m$^3$), respectively; however, $(1/2)MgH_2$ is a product of the hydrogenation reaction together with $CuLi_{0.08}Mg_{1.42}H_4$ enhancing its capacity to that of $CuLi_{0.08}Mg_{1.92}H_5$ which has a gravimetric capacity of 4.4 wt% (110 kg/m$^3$). If molecular hydrogen is additionally stored, the gravimetric capacity of $CuLi_{0.08}Mg_{1.92}H_5$ can increase to $CuLi_{0.08}Mg_{1.92}H_{5.5}$ (4.8 wt%, 120

kg/m$^3$), or $CuLi_{0.08}Mg_{1.92}H_6$ (5.2 wt%, 130 kg/m$^3$), respectively. The latter two compositions concern to the hydride that absorbed four or eight molecules of hydrogen per formula unit of $Cu_{16}LiMg_{23}H_{64}$, respectively.

*4.2.2 Inelastic Incoherent Neutron Scattering measurements*

Inelastic Neutron Scattering (INS) measurements were performed to determine the structure of the hydrides. INS is highly sensitive to the presence of hydrogen and, when associated with simulated PDOS, can bring valuable insights on the crystal structure and bonds of the hydrides.

Our calculations show that $CuLi_{0.08}Mg_{1.42}H_4 + (1/2)MgH_2$ is always more stable than $CuLi_{0.08}Mg_{1.92}H_5$. There is a small possibility that $CuLi_{0.08}Mg_{1.92}H_5$ (figure 3a) is formed by direct hydrogenation at -80 ºC from the hydrogen left in the crucible. Therefore, we think that $CuLi_{0.08}Mg_{1.42}H_4 + (1/2)MgH_2 \leftrightarrow CuLi_{0.08}Mg_{1.92}H_5$ takes place at low temperatures. $CuLi_{0.08}Mg_{1.92}H_5$ is observed in figure 3a and 3b in comparison with its theoretical PDOS showing a good agreement.

INS measurements and the phonon calculated vibration spectra in figure 3a and 3b show that $CuLi_{0.08}Mg_{1.92}H_5$ disproportionates to form $MgH_2$ as observed in figure 3c. This assumption proceeds from the verification that samples which did not initially contain $CuMg_2$ (like sample A), will also form $MgH_2$ after some hydrogenation cycles. For sample A, the formation of $MgH_2$ could only be due to the reaction: $2CuLi_{0.08}Mg_{1.42}H_4 + MgH_2 \leftrightarrow CuLi_{0.08}Mg_{1.92} + 5H_2$ (Table 2, reaction 1) since, in absence of $CuMg_2$, no other phase will generate $MgH_2$ as a product of its hydrogenation.

Moreover, $CuLi_{0.08}Mg_{1.42}H_4$ can also be observed in the 6$^{th}$ hydrogenation/dehydrogenation cycle, eventually denoting that $CuLi_{0.08}Mg_{1.42}H_4$ was frozen during quenching or that $CuLi_{0.08}Mg_{1.42}H_4 + (1/2)MgH_2 \leftrightarrow CuLi_{0.08}Mg_{1.92}H_5$ proceed to only a

small extent. $CuLi_{0.08}Mg_{1.42}H_4$ and $MgH_2$ are observed in the INS spectrum correspondent to the 6$^{th}$ hydrogenation/dehydrogenation cycle of sample A, reinforcing our assumptions on the formation of $CuLi_{0.08}Mg_{1.42}H_4$ and $MgH_2$ from $CuLi_{0.08}Mg_{1.92}H_5$ disproportionation. $CuLi_{0.08}Mg_{1.42}H_4$ possesses the only PDOS spectrum that justifies the vibration mode at 873 $cm^{-1}$, as shown in figure 3d.

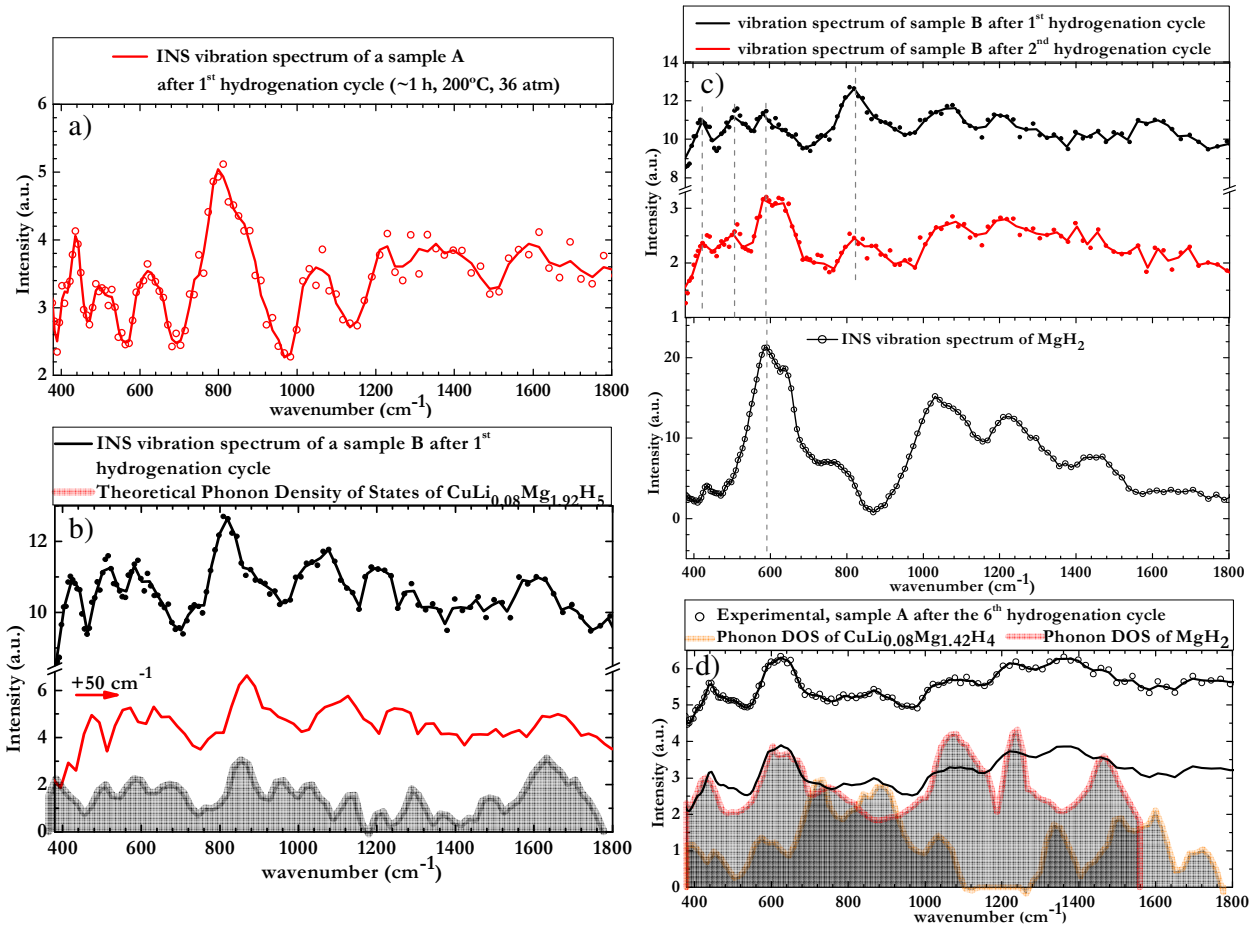


**Fig. 3 a)** Vibrational spectra of a sample A initially containing $CuLi_{0.08}Mg_{1.92}$ and $Cu_2Mg$ after being hydrogenated at 200 ºC at 36 atm for 1h15min (no activation cycles were performed) and measured at -263 ºC. **b)** Vibrational spectra of a sample B after one hydrogenation cycle at 15 atm, at 200 °C, for 24 h (no activation cycles were performed) and measured at -263 ºC in comparison with theoretical Phonon Density Of States (PDOS) obtained for $CuLi_{0.08}Mg_{1.92}H_5$. Regions with similar shapes can be observed, sometimes occurring at slightly different wavenumber ranges which is a common occurrence when DOS calculations are compared with experimental data. **c)** Comparison between the first and the second hydrogenation cycles performed on the same sample B. It is possible to identify the presence of $CuLi_{0.08}Mg_{1.92}H_5$ and $MgH_2$, meaning that a part of $CuLi_{0.08}Mg_{1.92}H_5$ was disproportionated into $CuLi_{0.08}Mg_{1.42}H_4$ and $MgH_2$. It is possible that the $CuLi_{0.08}Mg_{1.42}H_4$ correspondent spectrum is overlapped with the spectra of $CuLi_{0.08}Mg_{1.92}H_5$ and $MgH_2$. **d)** Vibration spectrum measured at -263 ºC, of a sample A after six hydrogenation cycles. It is likely that this spectrum is the superposition of the $CuLi_{0.08}Mg_{1.43}H_4$ and $MgH_2$ spectra. The calculated PDOS of $CuLi_{0.08}Mg_{1.42}H_4$ and $MgH_2$ are shown for comparison. The relative amounts of each phase, the incoherent cross-sections, and the overtones were not taken into account.

4.3 Samples A, B and F

*4.3.1 Sample A containing $Cu_2Mg$ and $CuLi_{0.08}Mg_{1.92}$*

This sample was studied both theoretically and experimentally. It functioned as a control sample for the study of the $CuLi_{0.08}Mg_{1.92}$ compound upon hydrogenation and it initially contained 77.5 wt% of $CuLi_{0.08}Mg_{1.92}$ and 22.5 wt% of $Cu_2Mg$ (82.5 at% of $CuLi_{0.08}Mg_{1.92}$ and 17.5 at% of $Cu_2Mg$).

*4.3.1.1 DSC/TGA measurements*

In figure 4, 1.8 wt% (1.4 wt%/0.775) of the hydrogen that can be released from the active sample (ignoring $Cu_2Mg$ that remains unreacted) were desorbed, corresponding to a 1.4 wt% drop in weight of the whole sample. This hydrogen desorption took place in approximately 20 min between 63 ºC and 100 ºC as observed in the DSC experiment performed at about 1 atm of Argon. Actually, it can be concluded that 74% of the stored hydrogen was released in 10 min, between 63ºC and 99 ºC.

The sample could have absorbed another 2.0 wt% of hydrogen from a maximum of 3.4 wt% = 4.4 wt% × 0.775. The sample was unlikely to be saturated since it is necessary a pressure of ~330 atm to hydrogenate $CuLi_{0.08}Mg_{1.92}$ phase in the pristine sample A at 200ºC (as will be demonstrated later in *4.3.1.3* by observation of the Van't Hoff plot). To use moderate pressures, lower temperature should have been used. It is possible that this sample was hydrogenated during the heating and cooling processes in the $H_2$ atmosphere at ~110 atm.

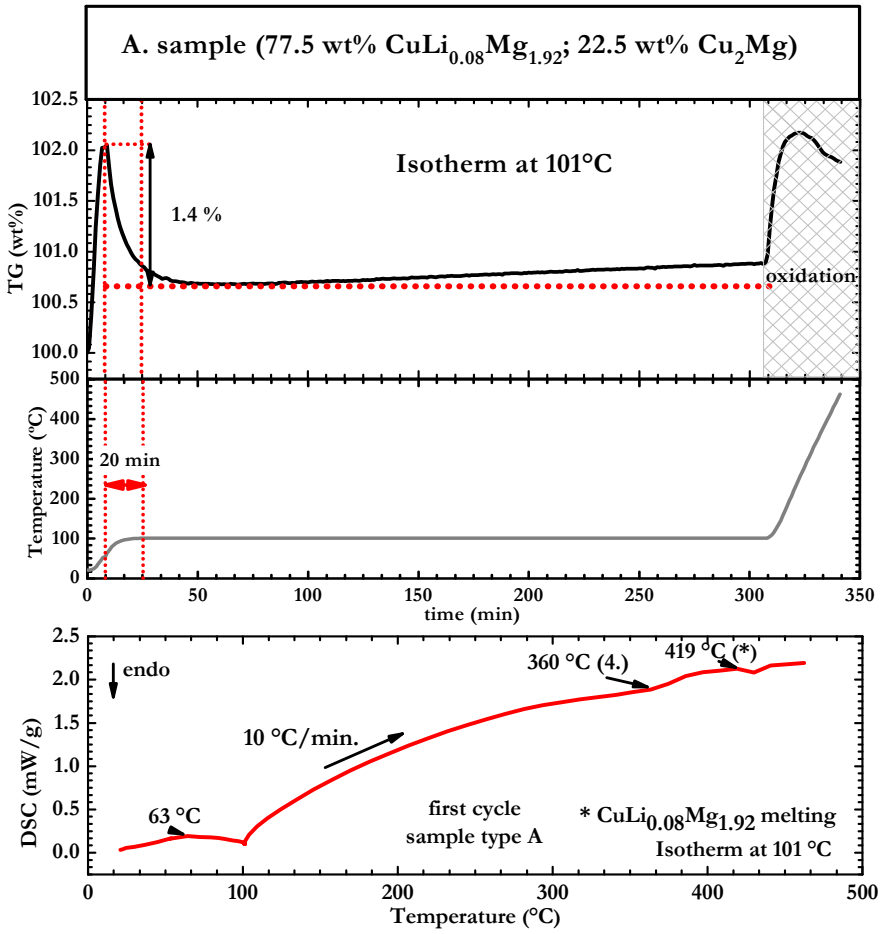


**Fig. 4.** DSC/TGA isotherm of sample A at 101 °C. Until the 101 ºC were reached, the heating rate was ~5 °C/min. It can be observed that before the thermal equilibrium is reached at 101 °C, mass drops 1.4 % starting at 63 °C. It can also be inferred from the DSC vs. temperature diagram that two other endothermic reactions occur at 360 °C and 419 °C, respectively. The first should correspond to $MgH_2$ decomposition and the second to $CuLi_{0.08}Mg_{1.92}$ melting point. Moreover, if the major part of $CuLi_{0.08}Mg_{1.42}H_4$ is converted into $CuLi_{0.08}Mg_{1.92}$ and $H_2$, then reaction 2, 3 and 4 (in Table 2) do not occur or occur in a very small extent as observed in this experiment. As $Cu_2Mg$ will not react, in this cycle, 1.8 wt% of hydrogen was absorbed by the active sample.

The DSC/TG curve of sample A in figure 4 may exhibit endothermic peaks corresponding to all the reactions in Table 2 if the heating rate and phases concentrations do not allow for

complete reactions. If desorption completion is allowed, only the first reaction of Table 2 will take place, as observed in figure 4.

*4.3.1.2 XRD measurements*

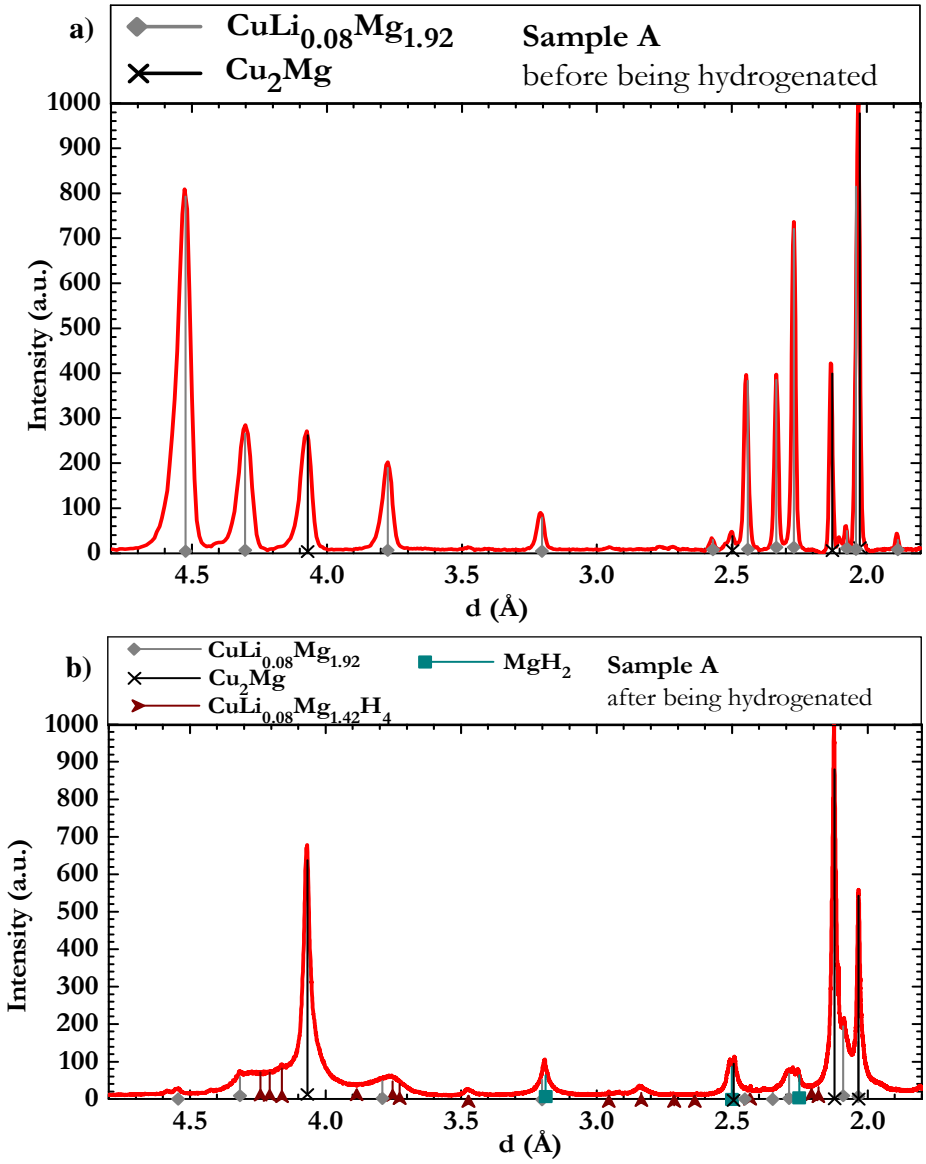


**Fig. 5** XRD Diffractograms of a sample A initially containing (77.5 wt% $CuLi_{0.08}Mg_{1.92}$ and 22.5 wt% $Cu_2Mg$). After hydrogenation the presence of $CuLi_{0.08}Mg_{1.42}H_4$ and $MgH_2$ is observed. **a)** pristine sample measured at the laboratory instrument. **b)** hydrogenated sample measured at 11-BM, APS, Argonne ($\lambda$ = 0.413570 Å). The sample presented the phases $Cu_2Mg$ + $MgH_2$ + $CuLi_{0.08}Mg_{1.42}H_4$ and $CuLi_{0.08}Mg_{1.92}$ (probably a solid solution in which some hydrogen is dissolved). Although the sample seemed saturated it should have desorbed some hydrogen before the experiment at the synchrotron, or during transportation, and this is why $CuLi_{0.08}Mg_{1.92}$ was observed.

In figure 5**,** XRD diffractograms show the formation of $MgH_2$ in a sample A (Table 1 and figure 1) - with 77.5 wt% of $CuLi_{0.08}Mg_{1.92}$ and 22.5 wt% of $Cu_2Mg$ upon hydrogenation. The sample can be observed after the second hydrogenation cycle (figure 5b), in which $CuLi_{0.08}Mg_{1.92}$ is reduced to a residual presence. The other phase present is $CuLi_{0.08}Mg_{1.42}H_4$. XRD diffractogram in figure 5b shows the presence of $CuLi_{0.08}Mg_{1.42}H_4$, although due to the amount of hydrogen present in $CuLi_{0.08}Mg_{1.42}H_4$ and since hydrogen does not scatter light well, the phase's percentage cannot be determined with accuracy.

*4.3.1.3 Van't Hoff plot and absorption measurements*

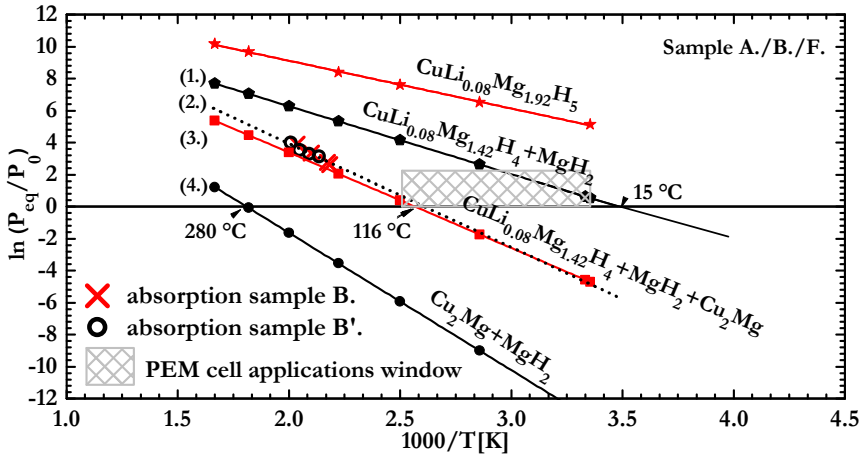


**Fig 6.** Calculated Van't Hoff plots after the reactions in Table 2 for three different samples of Table 1. In addition to calculated data, it is shown the experimental P-C-T data for two samples B and B' with different compositions. The equilibrium pressure of these samples at different temperatures was determined during hydrogen absorption. It can be observed that the experimental data (and linear fitting – dotted line) is very close to the straight line with squares that represents reaction 2 in Table 2, as expected. There are two reactions within the PEM fuel cells application range.

The Van't Hoff plot in figure 6 shows the calculated equilibrium pressures for samples A, B and F, at different temperatures. In fact, the equilibrium pressures reflect the reactions in Table 2. Absorption data was additionally obtained in a Sieverts-like instrument with two samples B with different compositions (B and B'), which are going to be presented in detail in 4.3.2. Samples were neither heat treated nor cycled before the absorption experiment. At a

certain temperature, samples absorbed hydrogen until equilibration. The corresponding equilibrium pressures are shown in figure 6.

*4.3.1.4 INS measurements*

A sample A, hydrogenated at 36 atm may only absorb hydrogen at ~109 ºC or below this temperature, according to the reaction $2CuLi_{0.08}Mg_{1.92} + 5H_2 \rightarrow 2CuLi_{0.08}Mg_{1.42}H_4 + MgH_2$ observed in the Van't Hoff plot in figure 6. Sample A was hydrogenated at 200 ºC for 1h15min. However, for the aforementioned reasons, it must only have absorbed hydrogen during heating and cooling (at T ≤ ~109 ºC). After hydrogenation the sample was quenched to -263 ºC (the quenching process was performed in the INS instrument and lasted for ~2 h). INS experiments showed the presence of the $CuLi_{0.08}Mg_{1.92}H_5$ hydride as it can be observed in figure 3a. No other hydride is visible. Note that reaction 2 in Table 2 could not have occurred before the first dehydrogenation of sample A, since this pristine sample did not contain $CuMg_2$.

In figure 7, see also [43], it can be observed that the first hydrogenation cycle spectra for sample A and B are very similar to those we've obtained for a sample containing only the low temperature monoclinic $NiMg_2H_4$ phase; thus indicating similarity between the two crystal structures. This finding was not only experimentally verified; our calculations provided the same conclusions after scrutinizing several possibilities [43].

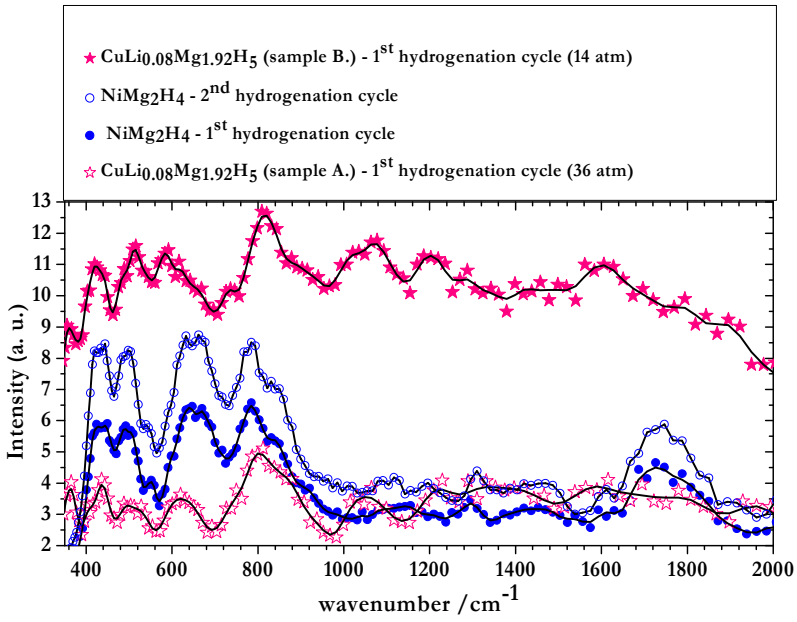


**Fig. 7** Vibration spectrum of a sample A and B after the first hydrogenation cycles in comparison with the $NiMg_2H_4$ – low temperature (LT) monoclinic *C2/c* structure $[NiH_4]Mg_2$ vibration spectra, after the first and second cycles. It can be observed a clear resemblance between the spectra of samples A, B and $NiMg_2H_4$ – LT indicate that the structure of these hydrides is similar. No significant difference is found between the 1st and 2nd hydrogenation cycles for $NiMg_2H_4$, as expected.

In summary, with experiments performed with sample A we were able to show that $CuLi_{0.08}Mg_{1.92}H_5$ disproportionates to form $CuLi_{0.08}Mg_{1.42}H_4$ and $MgH_2$. Reaction 1 of Table 2 was also verified using different techniques like DSC and XRD. $Cu_2Mg$ remains unreacted upon hydrogenation, as expected.

*4.3.2. Sample B containing $Cu_2Mg$, $CuLi_{0.08}Mg_{1.92}$ and $CuMg_2$*

Samples B belonging to a three phase equilibrium region of the phase diagram in figure 1, can be easily synthesized. Several samples B were prepared with different compositions.

*4.3.2.1 XRD measurements*

The expression of reaction 2 in Table 2 is observed not only in figure 6, highlighted in the results obtained after pressure-composition-temperature (PCT) experiments that were performed

with two different samples of the B type (B and B′), but also in figure 8. This figure shows the XRD of a sample B before and after being hydrogenated at 200 ºC and 102 atm. The sample was almost saturated with hydrogen although it was transported to the XRD instrument after cooling down (in the same hydrogen atmosphere), which might have led reaction 1 to move the thermodynamic equilibrium in the sense of releasing hydrogen.

$CuLi_{0.08}Mg_{1.92}$ might not have been fully hydrogenated. Reaction 2 was proceeded to completion since this sample showed the clear presence of $CuMg_2$ before hydrogenation, but no clear signs of it after hydrogenation, as it may be analyzed in figure 8. In fact, samples A and B show very similar XRD diffractograms after hydrogenation in the previous described conditions. The most important difference is related with the final amount of $MgH_2$. Sample B included $CuMg_2$ in its pristine condition; therefore, much more $MgH_2$ is formed until $CuMg_2$ runs out as it can be observed from the comparison of figure 5 and 8.

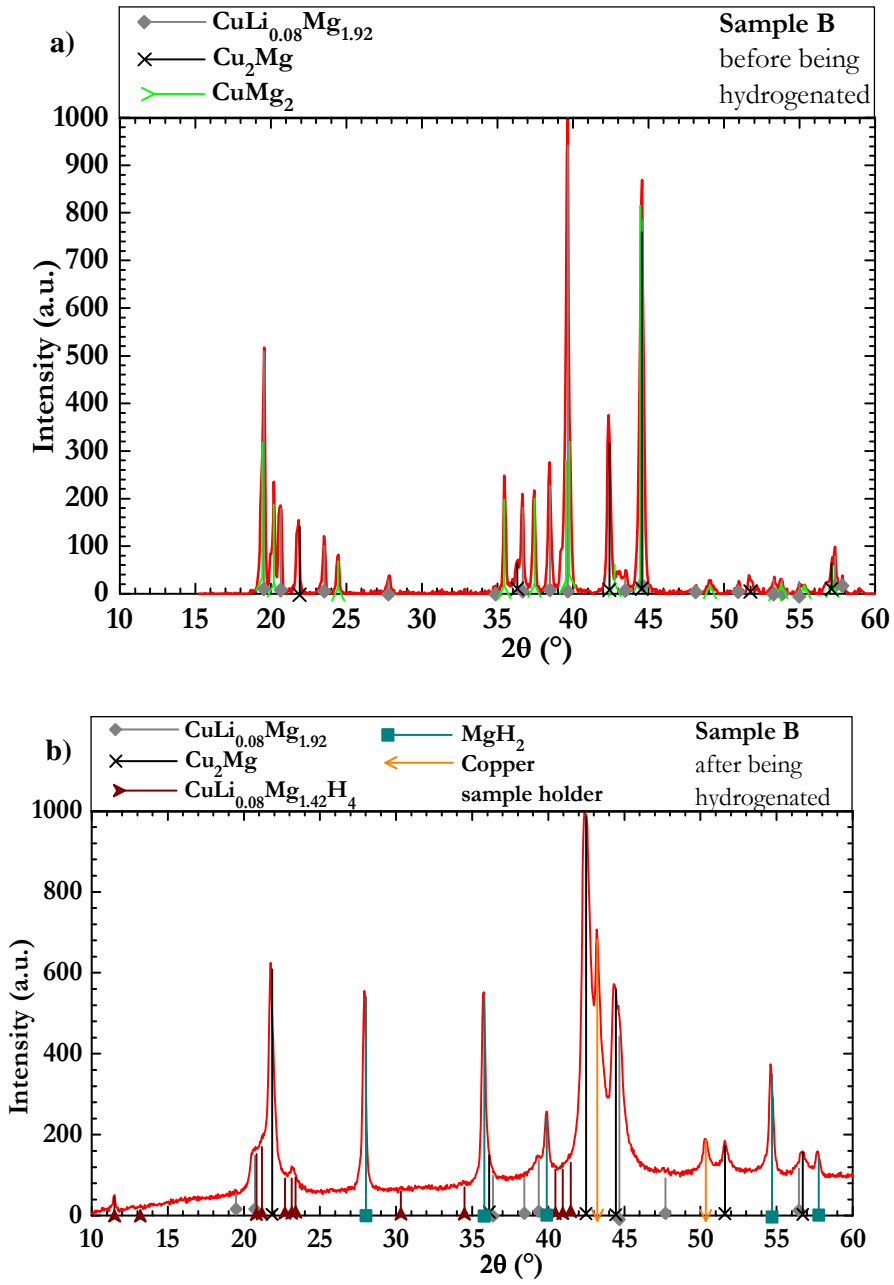


**Fig. 8** XRD diffractograms of a sample B initially containing (12.4 wt% $Cu_2Mg$, 60.0 wt% $CuLi_{0.08}Mg_{1.92}$, and 27.6 wt% $CuMg_2$). **a)** pristine sample. **b)** hydrogenated sample which presented the phases $Cu_2Mg + MgH_2 + CuLi_{0.08}Mg_{1.42}H_4$ and, eventually, $CuLi_{0.08}Mg_{1.92}$. As expected from the observation of Table 2, a sample B hydrogenated at 200 ºC and 102 atm is able to have all its $CuMg_2$ reacted and this is what we find in this diffractogram. Note that a small angle diffraction peak at $2\theta \sim 11.5°$ demonstrates the existence of holes in the crystal structure of $CuLi_{0.08}Mg_{1.42}H_4$.

*4.3.1.2 TG measurements*

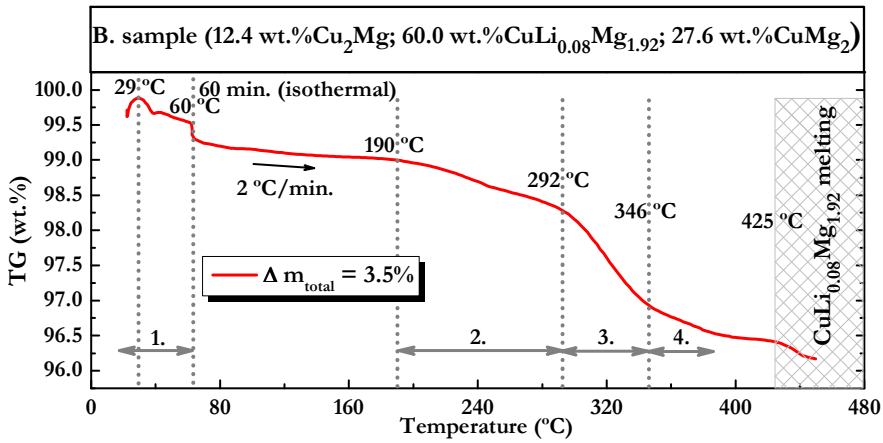


**Fig. 9** TG measurement of a sample B initially containing (12.4 wt% $Cu_2Mg$, 60.0 wt% $CuLi_{0.08}Mg_{1.92}$, 27.6 wt% $CuMg_2$) which was saturated with hydrogen prior to the experiment and was able to desorb 3.5 wt% of hydrogen. As $Cu_2Mg$ does not react, the sample desorbed 4.0 wt% of the active sample.

Figure 9 shows the TG curve for the sample B with 12.4 wt% $Cu_2Mg$, 60.0 wt% $CuLi_{0.08}Mg_{1.92}$, and 27.6 wt% $CuMg_2$ that was saturated with hydrogen. $Cu_2Mg$ will not be hydrogenated, or react with the other phases contained in the sample, as it can be observed in Table 2. The amount of hydrogen released was actually 4.0 wt% of the active sample (ignoring the amount of $Cu_2Mg$). Therefore, assuming that all $CuMg_2$ and $CuLi_{0.08}Mg_{1.92}$ will react, the amount of desorbed hydrogen is slightly higher than the calculated and would correspond to $CuLi_{0.08}Mg_{1.42}H_{\sim 4.4}$ which is roughly $CuLi_{0.08}Mg_{1.42}H_{4.5}$: the formula unit $Cu_{16}LiMg_{23}H_{64}$ plus 4 molecules of $H_2$. This discrepancy could also be associated with imprecisions in the percentage of the phases in the sample.

At this juncture, another effect that has to be accounted for is oxidation. The DSC apparatus is nearly depleted of oxygen; which would account for a decrease in the released mass. The amount of sample released near $CuLi_{0.08}Mg_{1.92}$ melting point was not factored in the calculation of $\Delta m_{total}$. Based on our findings, the prospective of having stored additional hydrogen in the molecular form is promising.

For sample A and B, reaction 2 occurring at 116 ºC in Table 2 seems to occur at much higher temperature in the DSC/TG curves (~190 ºC). Moreover, the experimental data plotted in the Van't Hoff plot in figure 6 is in agreement with the calculated temperature of reaction 2, indicating that this discrepancy is most likely due to the reaction kinetics or hysteresis in absorption/desorption cycles.

In summary, with sample B we could experimentally confirm all the correspondent reactions predicted in Table 2. From XRD measurements we could observe the presence of a hollowed structure, as expected to observe in $CuLi_{0.08}Mg_{1.42}H_4$ crystal structure.

*4.3.3 Sample F containing $CuLi_{0.08}Mg_{1.92}$ and $CuMg_2$*

This sample was not synthesized. Sample F is more efficient than A and B because it does not contain $Cu_2Mg$ that is kept unreacted during hydrogenation. It follows the same reactions scheme of samples A and B, as observed in Table 2. However, it is very difficult to synthesize since the $CuLi_{0.08}Mg_{1.92}$ + $CuMg_2$ equilibrium region is significantly narrow as shown in figure 1.

4.4 Samples C

Samples C contain a solid solution of Mg in Li, (Li), besides $Cu_2Mg$ and $CuLi_{0.08}Mg_{1.92}$. Therefore, they could have additional applications related with Li batteries. The presence of (Li) can help tailoring gravimetric capacities and desorption temperatures, since not only the amount of this phase can vary, but also its magnesium content. In the three phase region, however, the Mg content in (Li) cannot vary.

*4.4.1 Sample C containing (Li), $Cu_2Mg$, $CuLi_{0.08}Mg_{1.92}$.*

Lithium's solid solution (Li) was simulated as $Li_2Mg_3$ ~ $Li_{13}Mg_{19}$. A disordered supercell built from Li's crystal structure (body centered cubic, *Im-3m*), in which some of the Li atoms

were substituted by Mg atoms, was used to simulate (Li). According to the phase diagram in figure 1, $Li_2Mg_3$ stoichiometry is a good approximation for the content of Li and Mg in the (Li) phase in these samples.

In samples C, conversely to samples A, B and F, $Cu_2Mg$ will be active in the presence of (Li) and $CuLi_{0.08}Mg_{1.92}$. For these samples, there are two reactions of type 3 in Table 2; the difference among them will be the amount of hydrogen absorbed/released, temperature of the reaction, and the fact that Mg will be a product of hydrogenation at 177 ºC and $MgH_2$ at 203 ºC.

*4.4.1.1 DSC/TGA measurements*

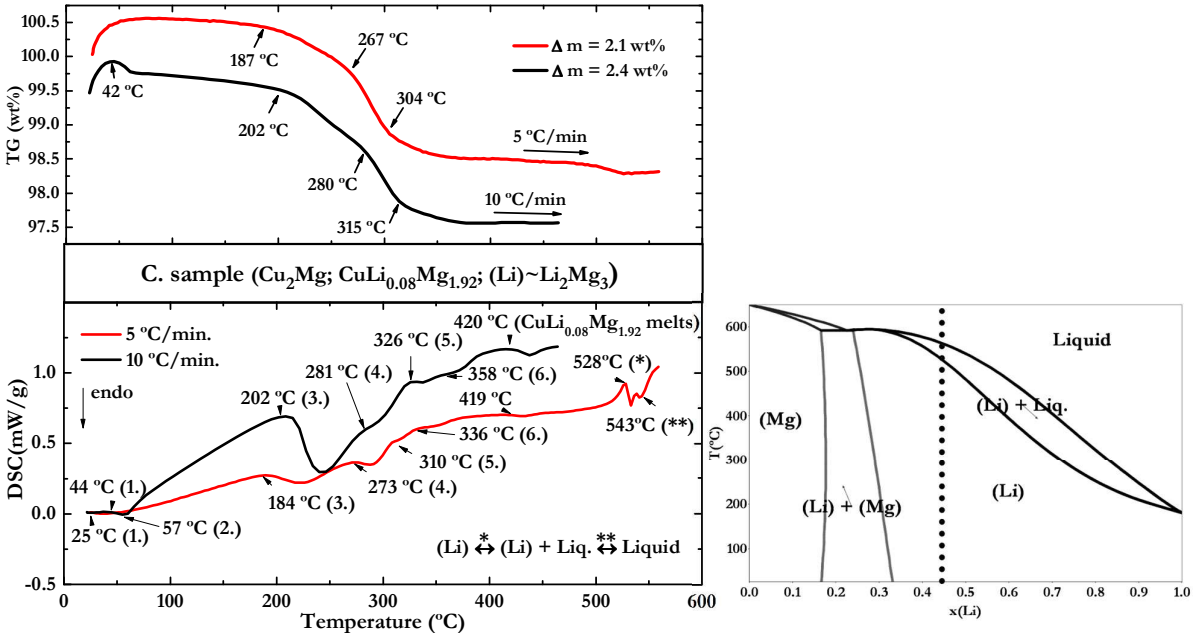


**Fig. 10** DSC/TG curves of two samples C with the same composition after being hydrogenated. The wt% of (Li) could not be determined with accuracy since Li does not scatter the x-rays well. Nevertheless, these measurements present high relevance to our study since every reaction of Table 2, for samples C, can be observed in these curves meaning that none of them was complete until reaction (6). The reactions (Li) → (Li) + Liq. → Liquid can be observed at 528 and 543 ° C, respectively. (Li) should correspond to a stoichiometry of about $Li_{0.44}Mg_{0.56}$ (highlighted in the binary phase diagram) which is approximately the composition of (Li) in the three phase region: $Cu_2Mg$ + $CuLi_{0.08}Mg_{1.92}$ + (Li) as can be observed in figure 1.

Figure 10 shows the TG and DSC curves of two samples C with the same composition. Heating rates were different for the two measurements (5 and 10 ºC/min). All correspondent

reactions in Table 2 seem to have occurred. The fact that the melting point of $CuLi_{0.08}Mg_{1.92}$ and $Li_2Mg_3$ (highlighted in the binary phase diagram of figure 10) could be observed, suggests good process reversibility.

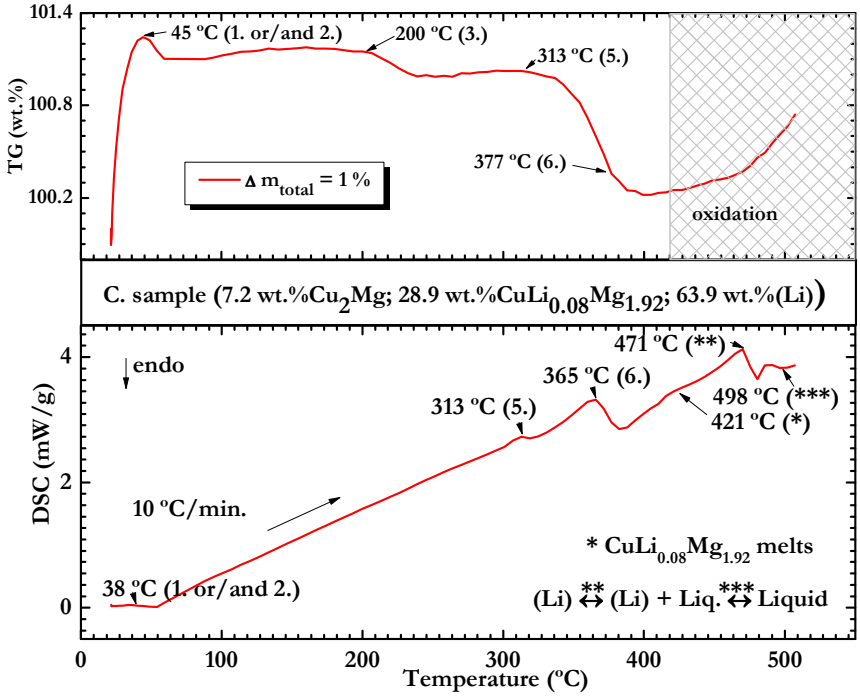


**Fig. 11** DSC/TG measurement of a sample C containing (7.2 wt% $Cu_2Mg$, 28.9 wt% $CuLi_{0.08}Mg_{1.92}$, 63.9 wt% (Li)), which was able to desorb 1.0 wt% of hydrogen. 60 wt% of (Li) did not react, as expected, from calculations presented in Table 2. The sample was saturated at the beginning of the measurement.

Sample C in figure 11 had initial composition of 63.9 wt% (Li), 7.2 wt% $Cu_2Mg$, and 28.9 wt% $CuLi_{0.08}Mg_{1.92}$. An important part of the (Li) phase in this sample remains inactive (it does not react) when the hydrogenation occurs at 200 ºC even if the sample cools down under an adequate pressurized hydrogen atmosphere. During hydrogenation, reaction 3 (C.) in Table 2 takes place and all $Cu_2Mg$ in (63.9 wt% (Li), 7.2 wt% $Cu_2Mg$, and 28.9 wt% $CuLi_{0.08}Mg_{1.92}$) runs out. The gravimetric capacity of the sample is ~ 0.15 wt% and $CuMg_2$, LiH and Mg form. The latter products can react with more hydrogen for ¼ of the total gravimetric capacity of reaction 2. In fact, ¼($2CuMg_2 + 2LiH + 4Mg + 3H_2$), the products of reaction 3 except for

$CuLi_{0.08}Mg_{1.42}H_4$, can be furthermore hydrogenated in reaction 2. All Mg is consumed at this point but the gravimetric capacity of the sample only increased to ~ 0.18 wt%. The remaining $CuLi_{0.08}Mg_{1.92}$ then reacts with hydrogen to produce $CuLi_{0.08}Mg_{1.42}H_4$ + (1/2) $MgH_2$, reaction 1. If this last reaction is complete, the gravimetric capacity of the sample would be ~1 wt%, which corresponds to the $\Delta m_{total}$ (wt% hydrogen) released in the TG/DSC experiment and highlighted in figure 11. After the above mentioned hydrogenation process, this sample would present the following phases: $CuLi_{0.08}Mg_{1.42}H_4$, $MgH_2$, $Cu_2Mg$, $CuMg_2$, LiH and (Li) ~ $Li_2Mg_3$ which will be determined in the XRD pattern of sample C after hydrogenation, later in *4.4.1.4*. From the initial 63.9 wt% (Li) about 60.0 wt% (Li) remained unreacted.

*4.4.1.2 Van't Hoff plot*

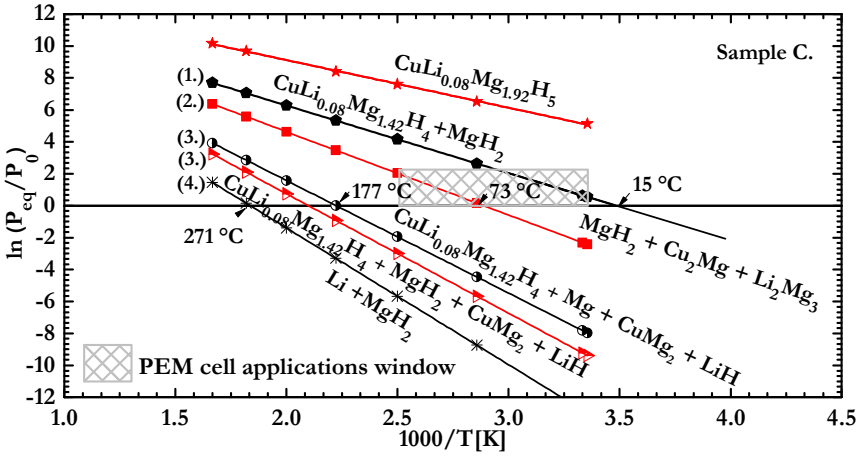


**Fig. 12** Van't Hoff plot for sample C for the calculated reactions in Table 2. There are two reactions within the PEM fuel cells application range.

Figure 12 shows that two of the sample C's reactions in Table 2 fall on the PEM fuel cell applications window. Nevertheless reaction 2, occurring at 73 ºC (1 atm), has a low gravimetric capacity (1.8 wt%), still higher than $LaNi_5H_6$ (~1.3 wt%) - a hydride with numerous practical applications but involving expensive elements.

Hydrogen absorption through reaction 2 can only take place after the hydrogenation corresponding to reaction 3 at 177 ºC, since there is no $CuMg_2$, LiH and Mg in the pristine sample C.

*4.4.1.3 INS measurements*

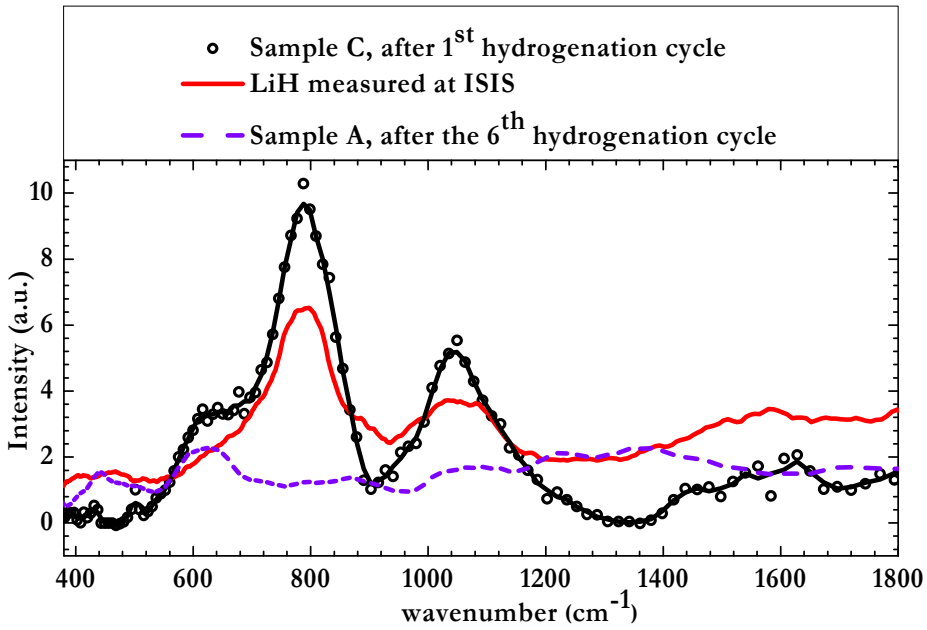


**Fig. 13** Vibration spectrum measured at -263 ºC, of a sample C containing LiH, $MgH_2$ and possibly $CuLi_{0.08}Mg_{1.42}H_4$ hydrides after one hydrogenation cycle at 200 °C, ~90 atm, for 15 h (no activation cycles were performed). Comparison between the hydrides of the different phases that comprise sample C after hydrogenation. Note: Sample A contains $MgH_2$ (most intense vibration mode at ~620 $cm^{-1}$). LiH spectrum was obtained in the ISIS database [44].

Figure 13 shows the INS vibrational spectra of a sample C that was hydrogenated just like in the previously described process and then quenched from room temperature to -263 ºC. At this temperature, the $CuLi_{0.08}Mg_{1.92}H_5$ hydride has been proved to be more stable than $CuLi_{0.08}Mg_{1.42}H_4 + (1/2)MgH_2$. However, the reaction $CuLi_{0.08}Mg_{1.42}H_4 + (1/2)MgH_2 \rightarrow CuLi_{0.08}Mg_{1.92}H_5$ may not have been complete and the hydrides would then be: $CuLi_{0.08}Mg_{1.92}H_5$, $CuLi_{0.08}Mg_{1.42}H_4$, $MgH_2$ and LiH. The latter two hydrides are easily identified in the vibration

spectra shown in figure 3 and 13. The characteristic frequencies of the vibration modes of the hydrogen bonds in $CuLi_{0.08}Mg_{1.92}H_5$ and $CuLi_{0.08}Mg_{1.42}H_4$ are mostly overlapping with those of $MgH_2$ and LiH making it more difficult to identify the first two hydrides.

*4.4.1.4 XRD measurements*

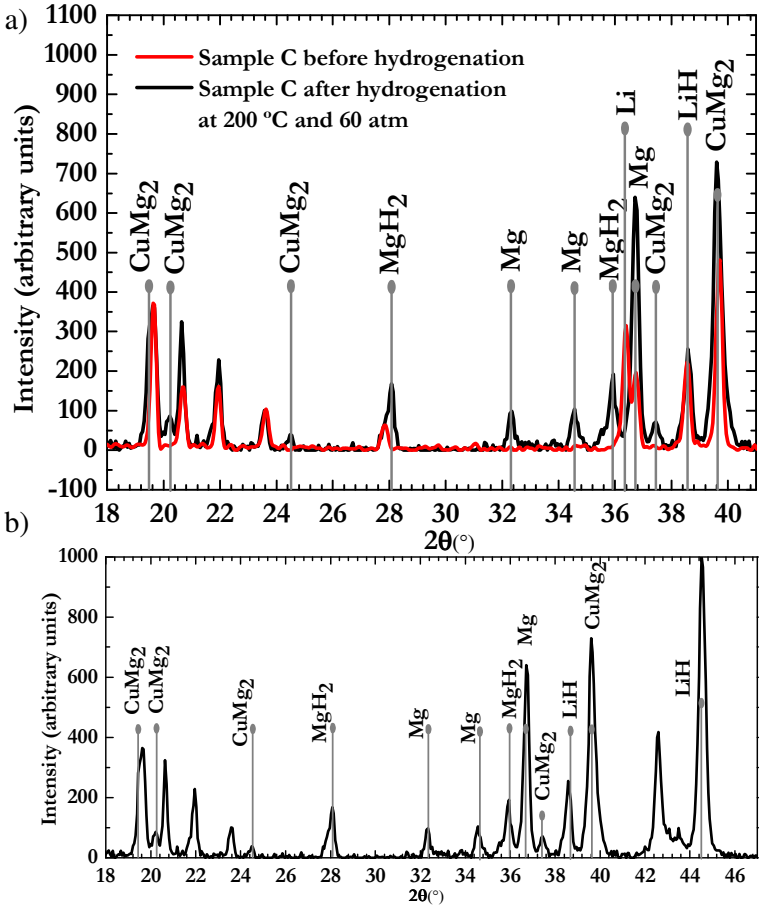


**Fig. 14** XRD for a sample C before and after hydrogenation. **a)** XRD pattern of a sample C initially containing $CuLi_{0.08}Mg_{1.92}$ + $Cu_2Mg$ + (Li) and that was hydrogenated at 200 °C, for 24 h, at ~ 60 atm (no activation cycles were performed). After hydrogen exposure, the XRD pattern shows $CuLi_{0.08}Mg_{1.42}H_4$, Mg, $MgH_2$, $CuMg_2$, and LiH that were not visible in the initial pattern. This is a clear demonstration that the reaction 3, at 177 ºC – 1 atm, took place. **b)** Extended diffractogram of sample C after hydrogenation. We have highlighted the Bragg peaks of select phases with the purpose of focusing on the reaction 3 associated phenomena.

In figure 14 sample C underwent hydrogenation at about 200 ºC, which is similar to the previously described process. Contrary to the DSC sample that released ~1 wt% of $H_2$, this one did not complete reaction 2 since Mg is still present. Reaction 1 was not completed as well, since $CuLi_{0.08}Mg_{1.92}$ is also detectable. This sample presented (Li), $Cu_2Mg$ and $CuLi_{0.08}Mg_{1.92}$ in its pristine form. Neither $CuMg_2$, nor Mg could be detected before hydrogenation. Note that (Li) ~ $Li_2Mg_3$ possesses the same crystal structure type as pure lithium, *Im-3m*. After hydrogenation the phases present were $CuLi_{0.08}Mg_{1.42}H_4$, $CuLi_{0.08}Mg_{1.92}$, $MgH_2$, $Cu_2Mg$, $CuMg_2$, LiH, Mg (hexagonal, *P6₃/mmc*), and eventually (Li). Li is very hard to identify with accuracy since it does not scatter light well. The same applies even further to hydrogen, as mentioned previously. The XRD diffractogram show that reaction 3, at 177 ºC, took place since the phases $CuLi_{0.08}Mg_{1.42}H_4$, $CuMg_2$, LiH, Mg are products of this reaction. Mg and $CuLi_{0.08}Mg_{1.92}$ did not run out and that means that reaction 2 and 1 were either not complete, evolved in the sense of releasing hydrogen, or did not take place at all.

In summary, sample C allowed the verification of all the corresponding hydrogenation/dehydrogenation reactions in Table 2. This is a remarkable achievement since we were able to find on the INS spectra and XRD diffractograms all of the products expected. LiH which was more difficult to find in a XRD pattern, is undoubtedly shown in the INS spectra.

In this sample, conversely to samples A, B and F, $Cu_2Mg$ will react with (Li) and $CuLi_{0.08}Mg_{1.92}$ at 177 ºC. This is another result to retain from these studies.

## 4.5 Samples D

### *4.5.1 Sample D containing (Li) and $CuLi_{0.08}Mg_{1.92}$*

This sample was not synthesized. Samples D suffer hydrogenation/dehydrogenation through reactions presenting the highest gravimetric capacities.

*4.5.1.1 Van't Hoff plot*

The concentrations of the two phases present in sample D can be used to obtain a tailored sample with gravimetric capacity between 4.4 - 5.0 wt% and decomposition temperatures at 15 ºC and 114 ºC (1 atm), as observed in figure 15. This is a value is especially significant, because their decomposition temperature falls within the proton exchange membrane fuel cell applications window. Likewise, the latter capacity can be most likely improved if physisorption capacity of $CuLi_{0.08}Mg_{1.42}H_4$ is used as well.

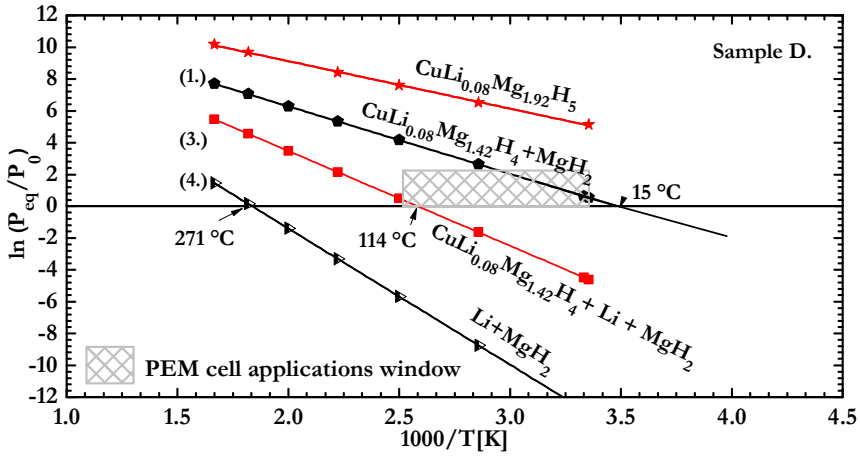


**Fig. 15** Van't Hoff plots after calculated reactions in Table 2 for sample D in Table 1. There are two reactions within the PEM fuel cells application range.

4.6 Samples E

*4.6.1 Sample E containing (Li), $CuLi_{0.08}Mg_{1.92}$ and $CuMg_2$*

This sample was not synthesized. Some of the reactions occurring in this sample upon hydrogenation are similar to those occurring with samples C. Note that besides reaction 1, reaction 3 at 160 ºC shows a gravimetric capacity of 4.0 wt% which might also be explored in the future.

4.7 The Li-Mg-H ternary $2Li + 3MgH_2 \leftrightarrow Li_2Mg_3 + 3H_2$ reaction

This reaction can take place in samples containing (Li), at 271 ºC - 1 atm. It was previously observed with sample C during a DSC/TG measurement shown in figure 10 (4). Nonetheless, this reaction occurs within the ternary: Li-Mg-H. It is within this system that the amount of Mg in the (Li) solid solution can be adjusted. The highest concentration of Mg in (Li) corresponds to the stoichiometry $Li_{0.33}Mg_{0.67}$; admitting that the thermodynamic parameters will not change much from those calculated for $Li_2Mg_3$ ~ $Li_{13}Mg_{19}$ ($Li_{0.41}Mg_{0.59}$), the decomposition temperature will rise to 280 ºC (1 atm) but the gravimetric capacity will also rise to 7.2 wt%, which is higher than the 6.5 wt% of $Li_2NH + H_2 \leftrightarrow LiNH_2 + LiH$ at 285 °C and 1 atm. Contrariwise, for example, for $Li_{0.45}Mg_{0.55,}$ the gravimetric capacity and decomposition temperature fall to 6.0 wt% and 263 ºC at 1 atm, respectively.

4.8 Application to Li batteries

One of the applications for this system is addressed by the work of Oumellal et al. [18]. This group worked with hydrides as negative electrodes. The presence of hydrogen enhances the diffusion properties of the electrode, avoiding polarization. We have hypothesized that a negative electrode made of $CuLi_{0.08}Mg_{1.42}H_4 + (1/2)MgH_2$, instead of just $MgH_2$, would be advantageous. An advantage of this system, which does not occur in the $MgH_2$ electrode, is related to the fact that no nano sizes are needed to produce $CuLi_{0.08}Mg_{1.42}H_4 + (1/2)\ MgH_2$ at room temperature. Moreover, $CuLi_{0.08}Mg_{1.42}H_4$ has higher electronic conductivity than $MgH_2$ [44] and it is well known that an electrode must be a good electronic conductor. To enhance conductivity and life cycle, Oumellal et al. [18] used $MgH_2$ nanopowders embedded in copper foam. The latter procedure has the obvious disadvantage of decreasing the specific capacity of the electrode.

The reaction occurring at the negative electrode would be: $CuLi_{0.08}Mg_{1.42}H_4 + ½ MgH_2 + 5Li^+ + 5e^- \leftrightarrow 5LiH + CuLi_{0.08}Mg_{1.92}$ with an equilibrium potential of $\Delta E_{eq} \sim 0.75$ V ($Li^+/Li^0$) calculated after Nernst equation: $\Delta E_{eq} = -\Delta G/nF$ where $\Delta G$ is the Gibbs free energy of the reaction, n the number of electrons and F the Faraday constant. This calculated value for $\Delta E_{eq}$ allows for all regular anode/cathode pairs. The theoretical specific capacity was calculated to be 1156 mAh/g (for negative electrode with 100% of $CuLi_{0.08}Mg_{1.42}H_4 + ½MgH_2$) which is much higher than the graphite's capacity of 372 mAh/g, the Li-ion battery negative electrode material.

Moreover, the structure in nanotubes of $CuLi_{0.08}Mg_{1.42}H_4$ will eventually facilitate Li-ion conduction which may be very relevant for these conversion batteries.

## 5. Conclusions

In summation, this research will open new vistas in the field of storage for both hydrogen and batteries. The Cu-Li-Mg-H catalytic system was presented in this study and its applications as a hydrogen storage material or negative electrode in Li batteries were addressed. In this study we were able to conclude the following:

1. Two hydrides will form upon $CuLi_{0.08}Mg_{1.92}$ hydrogenation, $CuLi_{0.08}Mg_{1.92}H_5$ (4.4 wt% and 110 kg/m$^3$ of hydrogen) which is stable at T < -80 ºC and $CuLi_{0.08}Mg_{1.42}H_4$ (3.9 wt% and 89 kg/m$^3$ of hydrogen) and will remain stable up to room temperature.
2. Extensive studies of this distinct family of hydrides via theoretical and experimental validations involving hydrogenation/dehydrogenation, have paved the way to innovative application opportunities, which could have far reaching implications. Reactions which enable many of these innovative applications are: $2CuLi_{0.08}Mg_{1.42}H_4 + MgH_2 \leftrightarrow 2CuLi_{0.08}Mg_{1.92} + 5H_2$ (4.4 wt% hydrogen, ~15 ºC), $2CuLi_{0.08}Mg_{1.42}H_4 + 2Li + 4MgH_2 \leftrightarrow 2CuLi_{0.08}Mg_{1.92} + Li_2Mg_3 + 8H_2$ (5.0 wt% hydrogen, ~114 ºC) and $2Li + 3MgH_2 \leftrightarrow Li_2Mg_3 + 3H_2$ (6.5 wt%

hydrogen, ~271 ºC). These reactions in toto occur in a sample containing (Li) and $CuLi_{0.08}Mg_{1.92}$ (sample D in this work).

3. The catalytic process in which $MgH_2$ can be formed at T > -80 ºC from $CuLi_{0.08}Mg_{1.92}H_5$ by disproportionation. In presence of $CuLi_{0.08}Mg_{1.42}H_4$, $MgH_2$ will release hydrogen at ~15 ºC. LiH can be formed at 175 ºC when found (Li) in presence of $CuLi_{0.08}Mg_{1.92}$. Hydrogen desorption may occur at this same temperature following the reverse reaction.
4. The unique low cost structure of $CuLi_{0.08}Mg_{1.42}H_4$ nanotubes, allows for the diffusion/storage of $H_2$ or $Li^+$. If four molecules per unit cell of $CuLi_{0.08}Mg_{1.42}H_4$ are absorbed, $CuLi_{0.08}Mg_{1.42}H_{4.5}$ (4.4 wt% and 100 kg/m$^3$ of hydrogen) will be formed. If eight molecules are absorbed, $CuLi_{0.08}Mg_{1.42}H_5$ (4.9 wt%, 112 kg/m$^3$ of hydrogen) is formed. The unit cell corresponds to $Cu_{16}LiMg_{23}H_{64}$.
5. The kinetic properties of this family of materials show very fast hydrogen absorptions/releases, e.g. 74% of the sample's total hydrogen released in 10 min. Samples of the material can be hydrogenated in less than one hour at a hydrogen pressure of ~50 atm and at temperatures lower than 200 ºC. We have also concluded that unlike other metal hydrides, no activation cycles are required for this unique family of $CuLi_{0.08}Mg_{1.42}H_4$ and $CuLi_{0.08}Mg_{1.92}H_5$ hydrides.

From the analysis of the equilibrium regions and correspondent hydrogenation reactions, it is possible to tailor the best sample in view of a practical application.

This work provides insight into a new and promising family of materials which holds the potential to be deployed into numerous energy storage saving applications. This research also involved the development of predictive strategies to assist in the discovery of materials at the atomic scale and the processes to control the nano and microscopic structures.

**Acknowledgements**

MHB would like to acknowledge FCT – Portugal and the FEDER - EU, for the PTDC/CTM/099461/2008 and PEst-C/EME/UI0285/2013 projects. This work has benefited from the use of FDS at LANSCE, Los Alamos National Laboratory, funded by DOE, DE-AC52-06NA25396 and from the use of 11-BM-B at the APS, Argonne National Laboratory.

MHB would like to acknowledge A Murchison - PATHION - for helpful discussions while writing this work and LL Daemen - Instrument Scientist of FDS - for his support while performing experimental work.

**References**

[1] A. Satheeth, P. Muthukumar, *Appl. Therm. Eng.* **2010**, *30,* 2698.

[2] K. Kurosaki, T. Maruyama, K. Takahashi, H. Muta, M. Uno, S. Yamanaka, *Sensors and Actuators* A. **2004**, *13*, 118.

[3] P. Muthukumar, M. Groll, *Int. J. Hydr. Ener.* **2010**, *35*, 3817.

[4] M. W. Rutherford, *Mater Sci. Forum*. **1988**, *31*, 19.

[5] Y. Liu, H. Pan, M. Gao, Q. Wang, *J. Mater. Chem.* **2011**, *21*, 4743.

[6] G. G. Libowitz, *J. Phys. Chem. Solids*. **1994**, *55* (12) 1461.

[7] G. Sandrock, *J. Alloys Compds.* **1999**, *293-295*, 877.

[8] NRPCT Letter MDO-723-0049. *Space Shielding Materials for Prometheus Applications*, Jan. 20 **2006**.

[9] F. H. Welch, *Nuclear Eng. and Design*, **1974**, *26* (3), 444.

[10] E. Veleckis, E. H. Van Deventer, M. Blander, *J. Phys. Chem.* **1974**, *78* (19), 1933.

[11] G.N. Lewis, *J. Am. Chem. Soc.* **1916**, *38*, 762.

[12] K. Moers, *Z. Anorg. U. All. Chem.* **1920**, *113*, 179.

[13] K. Peters, *Z. Anorg. U. All. Chem.* **1923**, *131*, 140.

[14] E. C. Potter, J. O'M. Bockris, *Colloques Intern. Centre Nat. Recherche Sci. (Paris), Eletrolyse.* **1952**, *39*, C3-C6.

[15] D. C. Bardwell, *J. Am. Chem. Soc.* **1922**, *44*, 2499.

[16] J. A. Plambeck, J. P. Elder, H. A. Laitinen, *J. Electrochem. Soc.* **1966**, *113 (9)*, 931.

[17] J. J. Vajo, F. Mertens, C. C. Ahn, R. C. Bowman, B. Fultz, *J. Phys. Chem. B,* **2004**, *108*, 13977.

[18] Y. Oumellal, A. Rougier, G. A. Nazri, J.-M. Tarascon, L. Aymard, *Nat. Mat.* **2008**, *7*, 916.

[19] J. C. R. E. Oliveira, M. H. Braga, *Appl. Phys. Lett.* **2013**, *103,* 23390.

[20] M. H. Braga, M. J. Wolverton, M. H. de Sá, J. A. Ferreira, *Neutron Diffraction*, (Ed: I. Khidirov), Intech, **2012** Ch. 1
http://www.intechopen.com/books/neutron-diffraction/hydrides-of-cu-and-mg-intermetallic-systems-characterization-and-catalytic-function

[21] I. Ansara, A. T. Dinsdale, M. H. Rand, (Ed. by) Database of the COST 507 project 2, **1998**, 170.

[22] a) M. H. Braga, *Degree Thesis*, University of Porto, 05, **1999**. b) M. H. Braga, L. F. Malheiros, M. Hämäläinen, *Thermochimica Acta*. **2000**, *344*, 47.

[23] Match, http://www.crystalimpact.com/, (accessed 09, 2013).

[24] P. M. Wolff, J. W. Visser, Absolute Intensities. Report 641.109. Technisch Physische Dienst, Delft, Netherlands. Reprinted: *Powder Diffract*. **1988**, ***3***, 202.

[25] P. Hohenberg, W. Kohn, *Phys Rev. B,* **1964***, 136*, 864.

[26] J. P. Perdew, Y. Wang, *Phys. Rev. B* **1992**, *45,* 13244.

[27] C. Colinet, *Intermetallics*, **2003**, *11*, 1095.

[28] P. E. Blochl, *Phys. Rev. B,* **1994**, 50, 17953.

[29] G. Kresse, J. Furthmüller, *Phys. Rev. B,* **1996**, *54*, 11169.

[30] K. Parlinski, Z. Q. Li, Y. Kawazoe, *Phys. Rev. Lett.* **1997**, *78,* 4063.

[31] NIST, Hydrogen, http://webbook.nist.gov/cgi/cbook.cgi?ID=C1333740&Units=SI&Mask=1#Thermo-Gas (accessed 09, 2013).

[32] J. J. Reilly, R. H. Wiswall, *Inorg. Chem.*, **1967**, *6* (12), 2220.

[33] J. J. Vajo, G. L. Olson, *Scripta Mat.* **2007**, *56*, 829.

[34] V. Hlukhyy, U. Ch. Rodewald, R. Pöttgen, *Z. Anorg. Allg. Chem.* **2005**, *631*, 2997.

[35] I. Ansara, A. T. Dinsdale, M. H. Rand, (Ed. by) Database of the COST 507 project 2, **1998**, 170.

[36] M. H. Braga, J. Ferreira, L. F. Malheiros, M. Hamalainen, *Z. Kristallogr. suppl.* **2007**, 26, 299.

[37] M. H. Braga, A. Acatrinei, M. Hartl, S. Vogel, Th. Proffen, L. L. Daemen. *J. Phys. Conf. Ser.* **2010**, *251*, 012040.

[38] M. H. Braga, J. A. Ferreira, M. Wolverton, *J. Therm. Anal. Calorim.* **2012**, *108*, 733.

[39] K. Yvon, G. Renaudin, *Encyclopedia of Inorganic Chemistry*, (Ed: R.B. King) Vol. III, **2006**, 1814.

[40] R. F. Lobo, M. Tsapatsis, C. C. Freyhardt, S. Khodabandeh, P. Wagner, C. Y. Chen, K.J. Balkus, S. I. Zones, M. E. Davis, *J. Am. Chem. Soc.* **1997**, *119* (36), 8474.

[41] DOE, Metal Hydride Hydrogen Storage R&D Activities http://www1.eere.energy.gov/hydrogenandfuelcells/storage/tech_status.html (accessed 09, 2013).

[42] Institut Néel CNRS, Stockage de l'hydrogène dans le magnesium http://neel.cnrs.fr/spip.php?article1281&lang=fr (accessed 09, 2013).

[43] G. D. Barrera, D. Colognesi, P. C. H. Mitchell, A. J. Ramirez-Cuesta, *Chem. Phys.* **2005**, *317* (2-3), 119.

[44] M. H. Braga, V. Stockhausen, M. Wolverton, J. A. Ferreira, J. C. E. Oliveira, *Mater. Res. Soc. Symp. Proc.* **2013,** 1496, doi:10.1557/opl.2013.375.